A gas pixel detector for x-ray polarimetry

Luca Baldini
INFN - Pisa

Why X-ray Astrophysical Polarimetry?

Polarization from celestial sources may derive from:

- Emission processes themselves:

  cyclotron, synchrotron, non-thermal bremmstrahlung

  (Westfold, 1959; Gnedin & Sunyaev, 1974; Rees, 1975

- Scattering on aspherical accreting plasmas:
  disks, blobs, columns.

  (Rees, 1975; Sunyaev & Titarchuk, 1985; Mészáros, P. et al. 1988)

- Vacuum polarization and birefringence through extreme magnetic fields

  (Gnedin et al., 1978; Ventura, 1979; Mészáros & Ventura, 1979)

Polarimetry would add to energy and time two further observable quantities, the amount and the angle of polarization, constraining any model and interpretation: a theoretical/observational breakthrough."

P. Meszaros et al. 1988

Polarization from Supernova Remnants: the Crab case

Radio
(VLA)

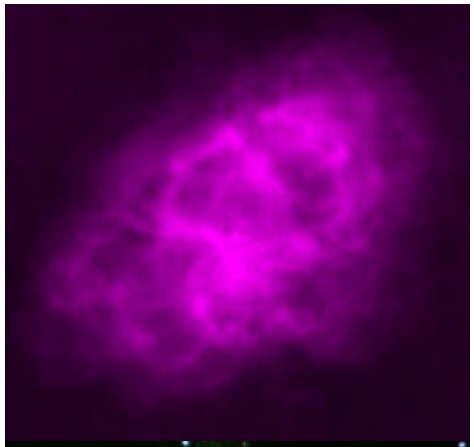

Infrared
(Keck)

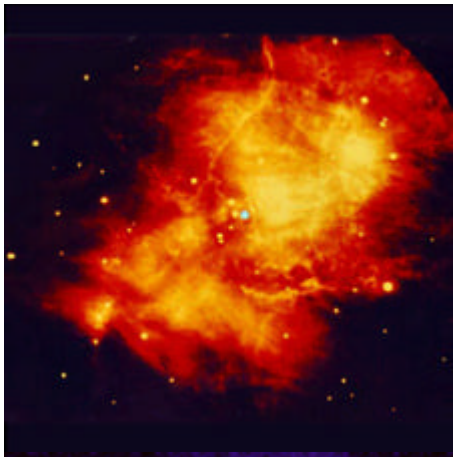

Optical
(Palomar)

X-rays
(Chandra)

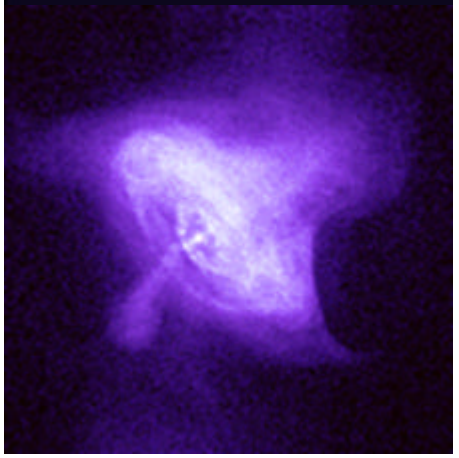

Crab-Nebula shows the same degree and angle of polarization from radio to X-rays and this is a signature of synchrotron emission.

Polarimetry: The Missing Piece of the Puzzle

Imaging: Chandra

Timing: RXTE

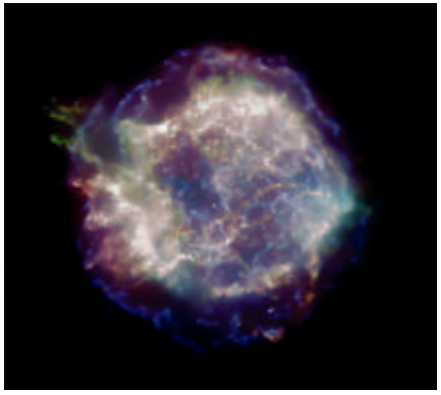

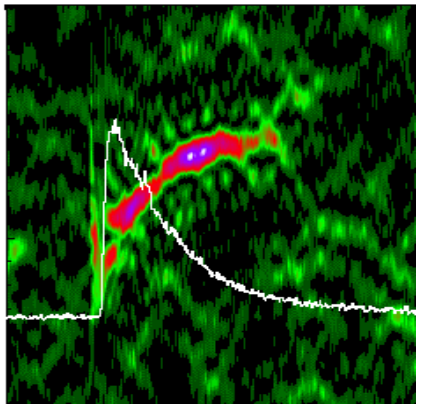

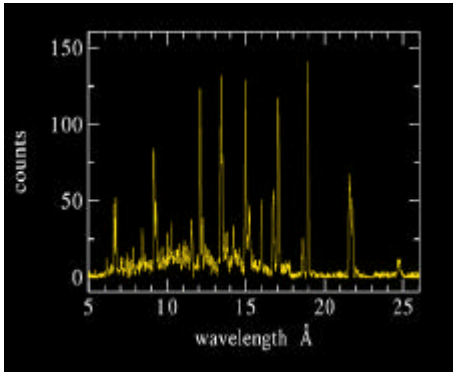

Spectroscopy: AstroE2, Constellation-X, Chandra

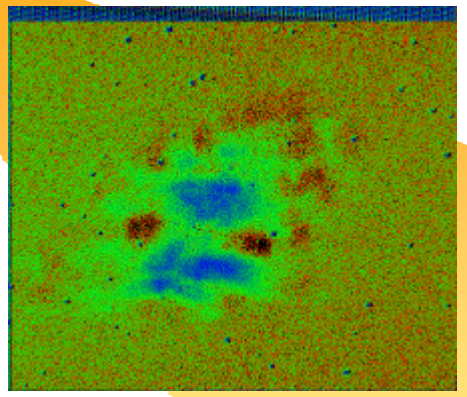

Polarimetry: AXP

Photoelectric cross section

The photoelectric effect is very sensitive to photon polarization!

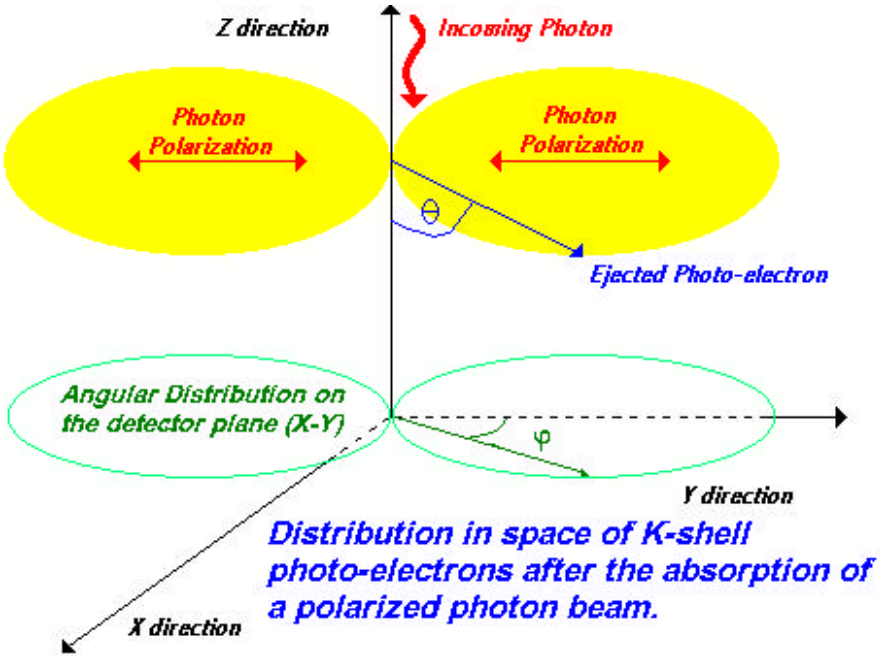

Distribution in space of K-shell photo-electrons after the absorption of a polarized photon beam.

Simple analytical expression for photoemission differential cross section (k-shell photoelectron in non-relativistic limit):

$$\frac{d\sigma}{d\Omega} \propto r_o^2 \frac{Z^5}{137^4} \left(\frac{mc^2}{h\nu}\right)^{7/2} \frac{4\sqrt{2}\sin^2\theta\cos^2\phi}{(1-\beta\cos\theta)^4}$$

If we project on the plane orthogonal to the propagation direction…

$$\frac{d\sigma}{d\Omega} \propto \cos^2\phi$$

Basics of photoelectric effect in gases

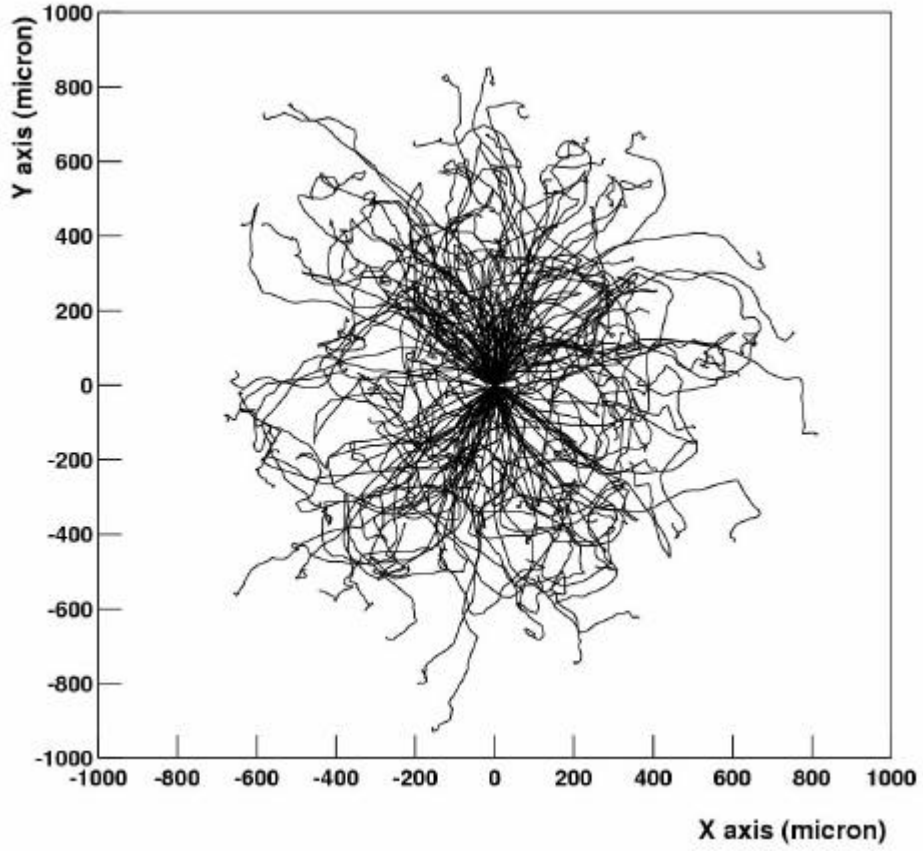

Slowing down:

$$\frac{?E}{?x} ? \frac{Z}{E}$$

Most of the energy is released at the end of the path.

Elastic scattering:

$$\frac{??}{??} ? \frac{Z^2}{E^2} \frac{1}{(\sin^2 \frac{?}{2} ? ?_{screen})^2}$$

Stopping power/Scattering ? 1/Z

Elastic scattering is responsible of a progressive randomization of photoelectron direction; most of the information about photoemission direction resides in the initial part of the track.

Basics of photoelectric effect in gas II

5.0 keV photoelectrons tracks in Ne (100% linearly polarized, collimated photons beam).

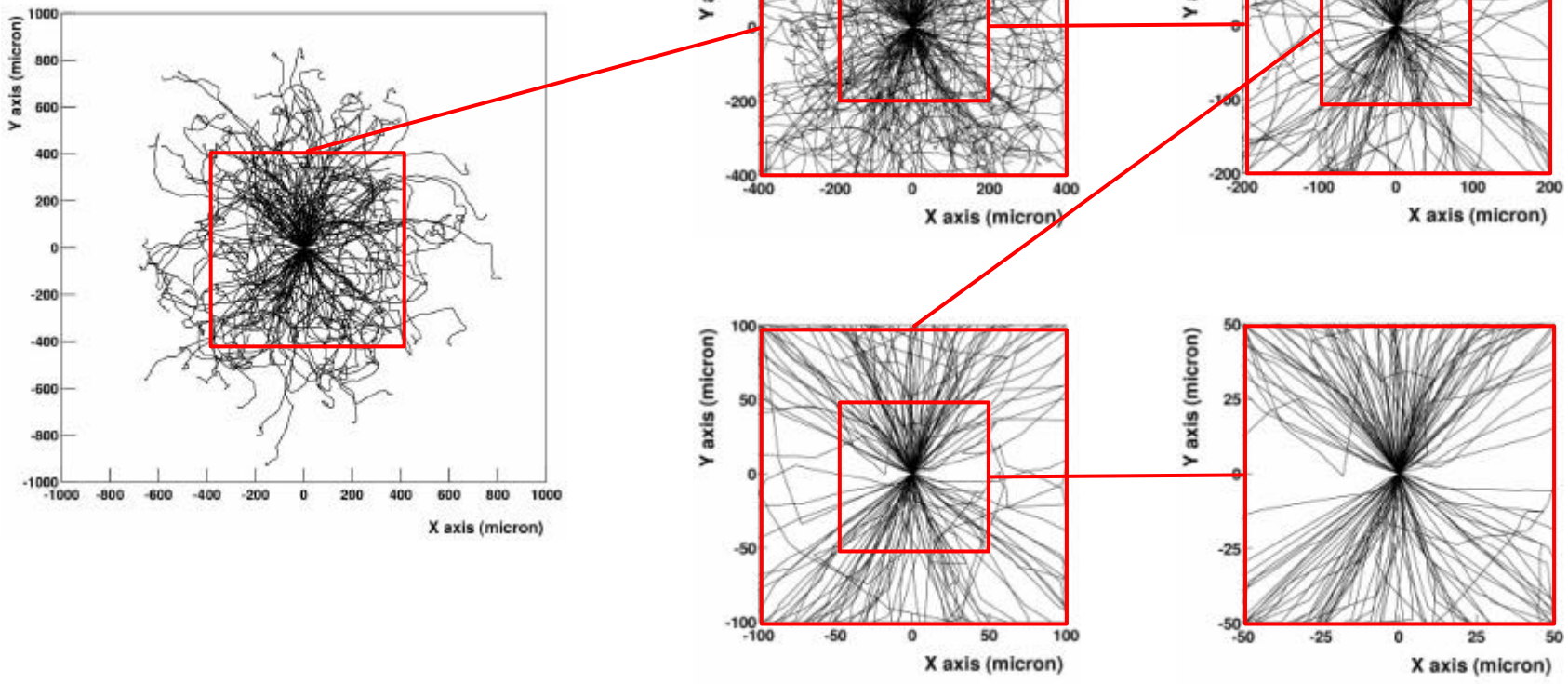

A precursor of full track imaging

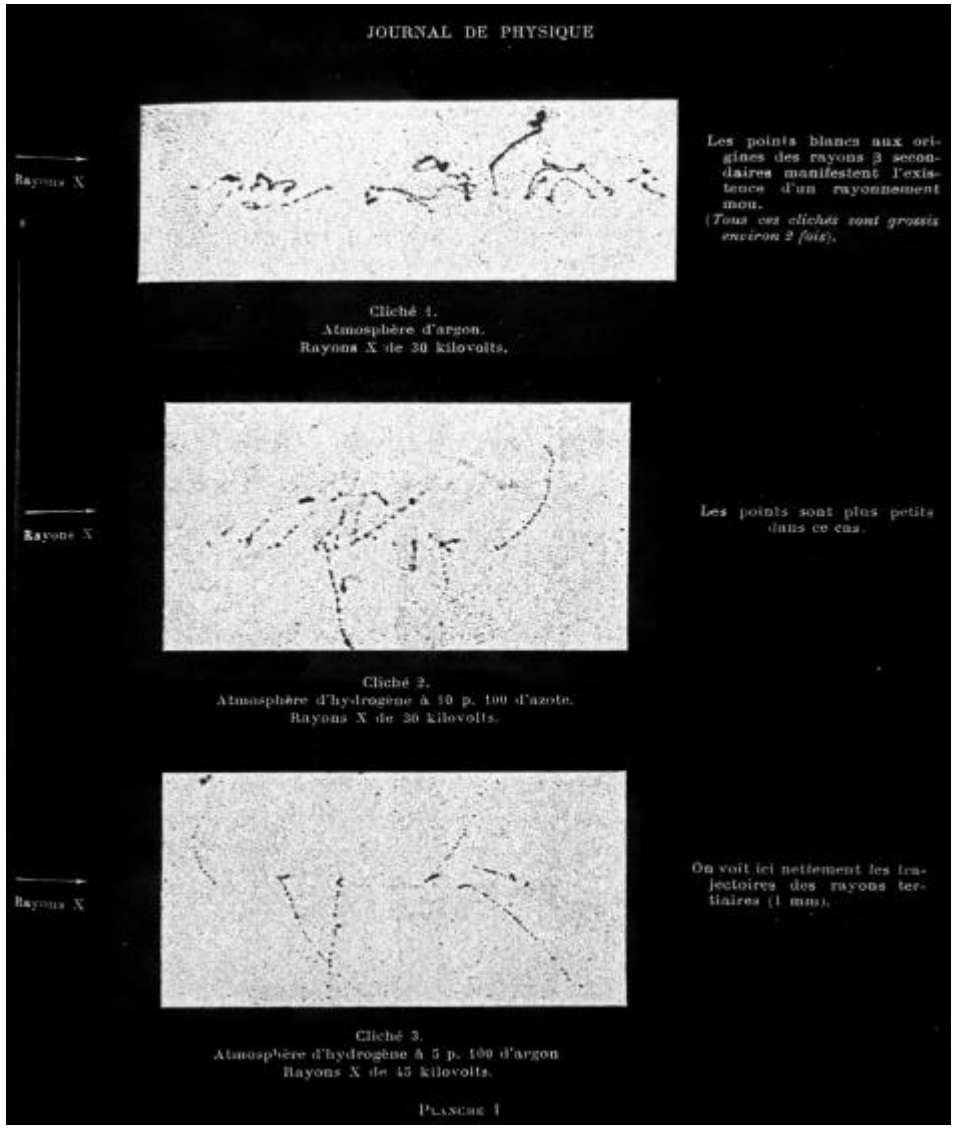
JOURNAL DE PHYSIQUE

Rayons X

Les points blancs aux origines des rayons β secondaires manifestent l'existence d'un rayonnement mou.
(*Tous ces clichés sont grossis environ 2 fois*).

Cliché 1.
Atmosphère d'argon.
Rayons X de 30 kilovolts.

Rayons X

Les points sont plus petits dans ce cas.

Cliché 2.
Atmosphère d'hydrogène à 10 p. 100 d'azote.
Rayons X de 30 kilovolts.

Rayons X

On voit ici nettement les trajectoires des rayons tertiaires (1 mm).

Cliché 3.
Atmosphère d'hydrogène à 5 p. 100 d'argon
Rayons X de 45 kilovolts.

PLANCHE I

P. Auger, 1926

30 keV photons in Ar

30 keV photons in H/N 90/10

45 keV photons in H/Ar 95/5

A “modern cloud chamber”: the Micro Pattern Gas Detector

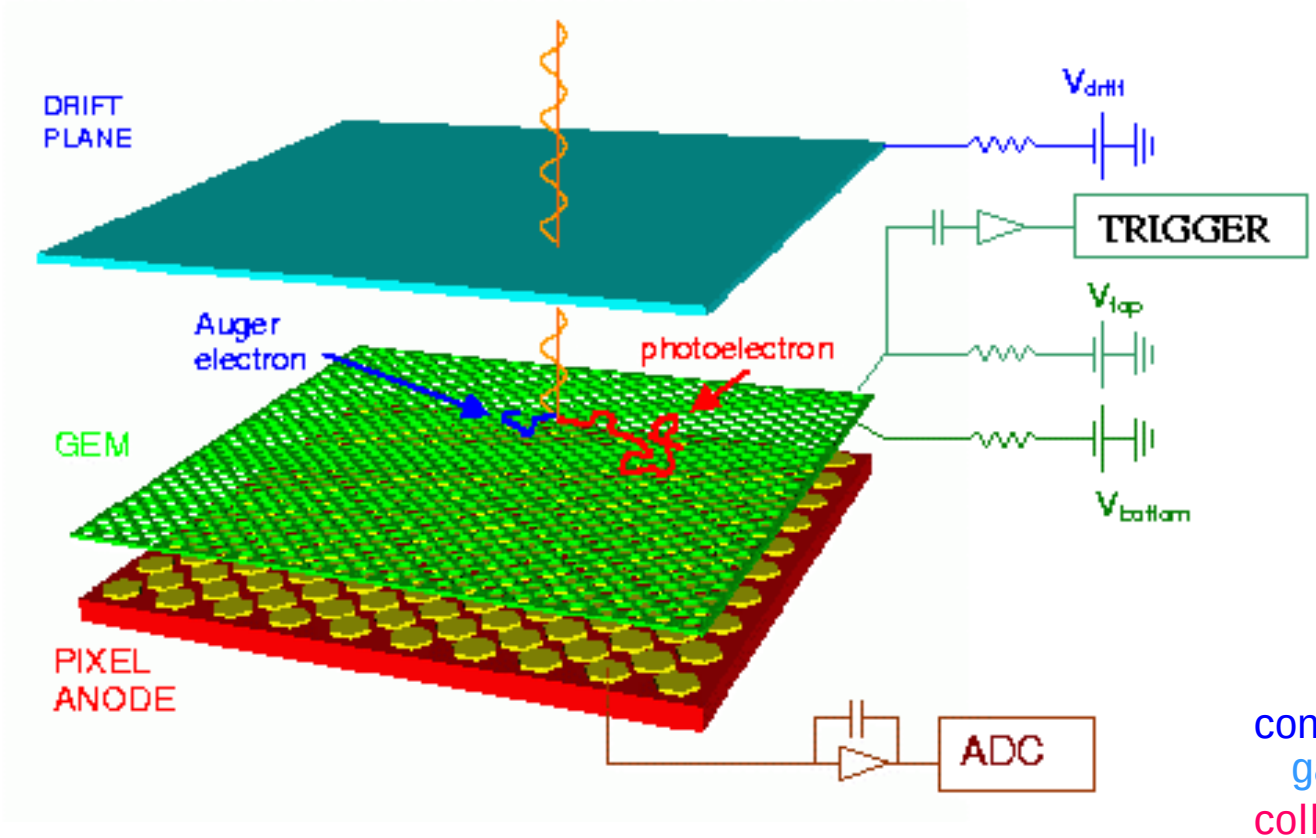

GEM electric field

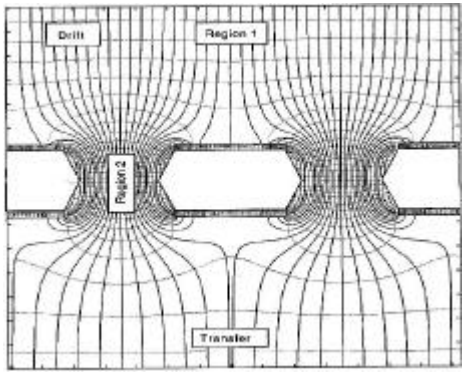

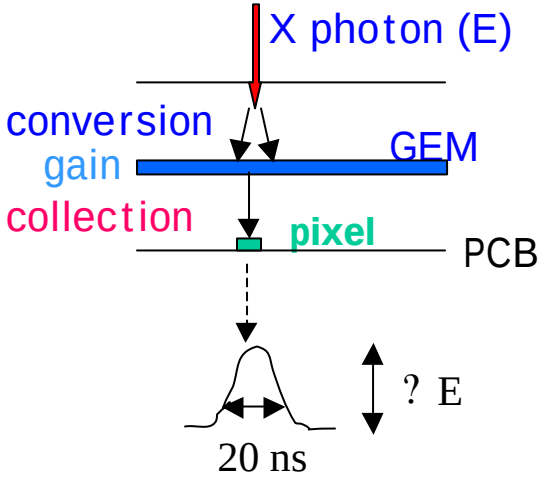

Polarization information is derived from the tracks of the photoelectron, imaged by a finely subdivided gas detector.

A first prototype: the PCB approach

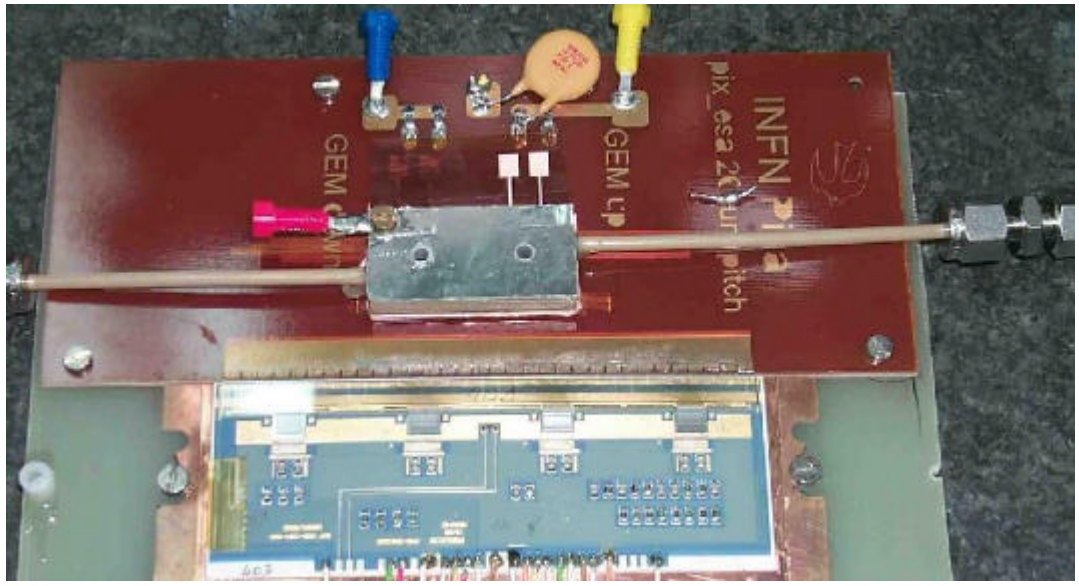

Gas electron Multiplier

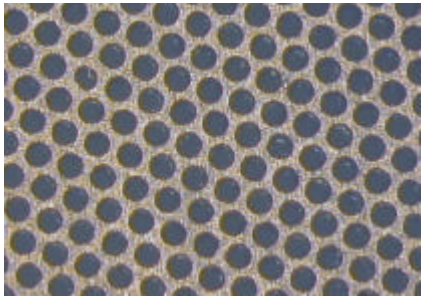

Read out plane

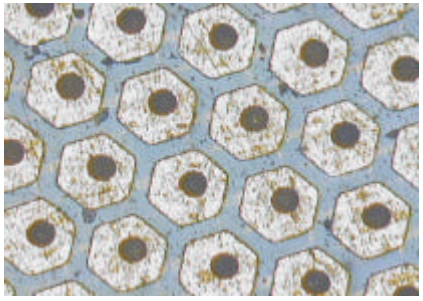

- GEM pitch: 90 ?m
- GEM thickness 50 ?m
- GEM holes diameters: 45 ?m, 60 ?m
- Read out pitch: 260 ?m
- Absorption gap thickness: 6 mm

512 electronic channels from a few mm^2 active area are individually read out by means of a multi-layer PCB fan out

Polarimetric sensitivity

5.9 KeV unpolarized source

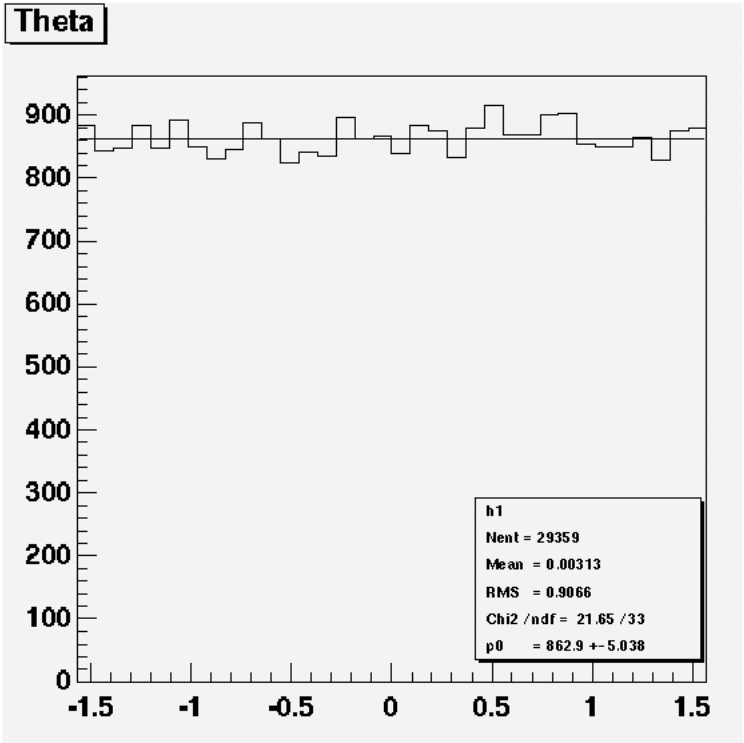

5.4 KeV polarized source

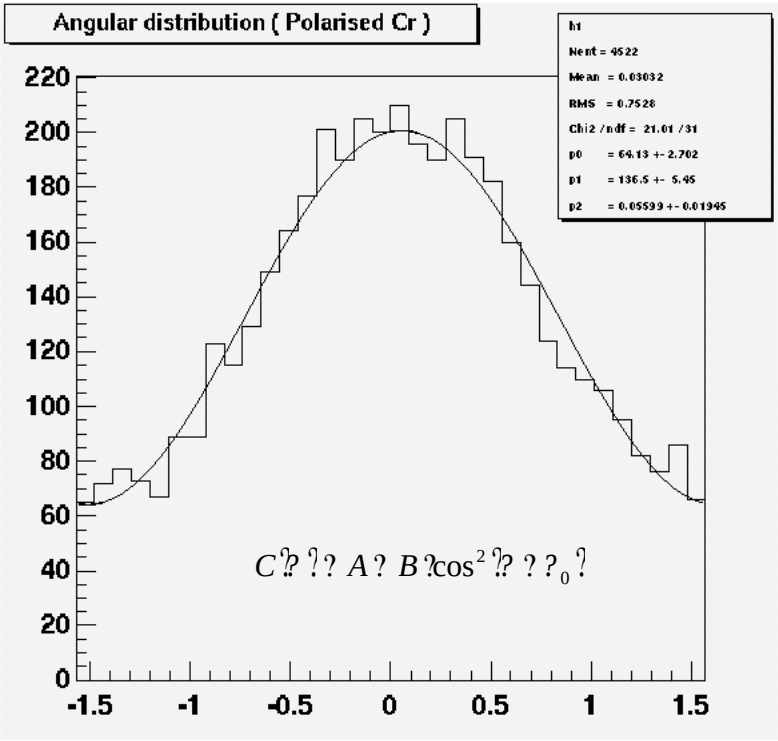

Modulation factor = (Cmax – Cmin)/ (Cmax + Cmin) ~ 50% at 6 KeV

$$MDP = \frac{1}{\mu} \cdot \frac{n_\gamma}{S} \cdot \sqrt{2\frac{S + B}{AT}}$$

MDP scales as: $1/\sqrt{\text{time}}$ for bright sources

$1/\text{time}$ for faint sources

The limits of the PCB approach

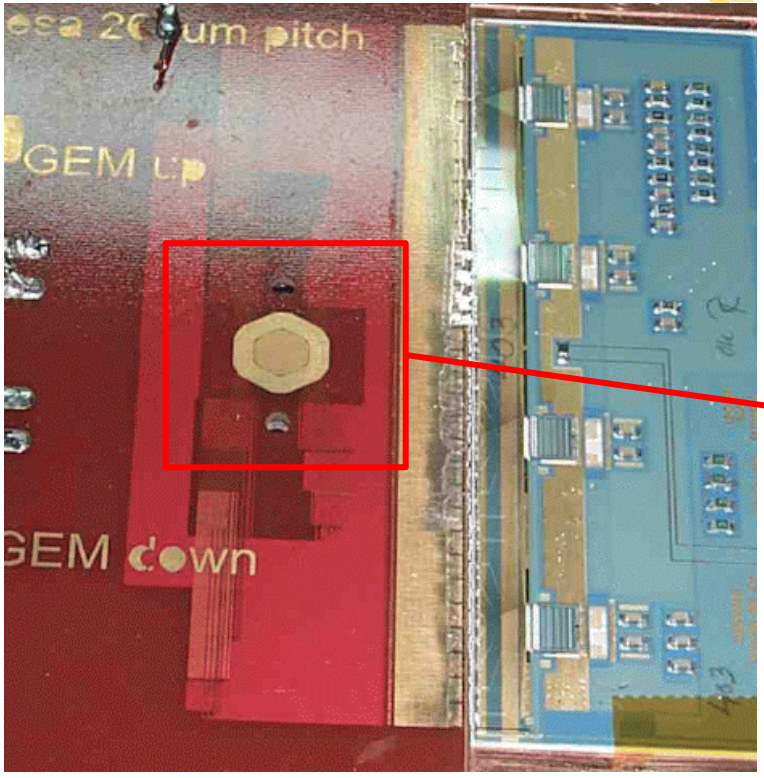

The fan-out which connects the segmented anode (collecting the charge) to the front end electronics is the real bottleneck!

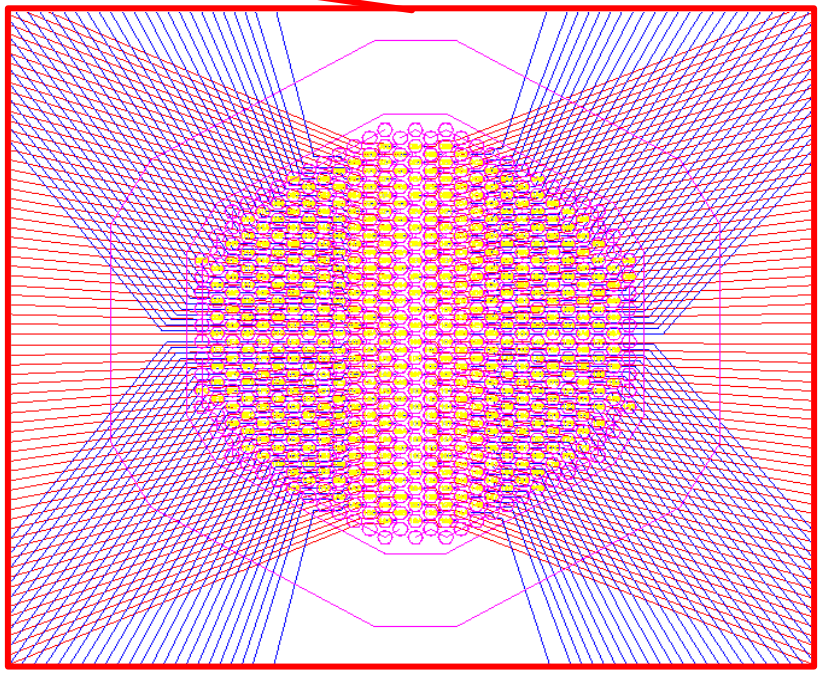

- Technological constraints limit the maximum number of independent electronics channels (~ 1000 @ ~ 200 ?m pitch).
- Crosstalk between adjacent channels (signals traveling close to each other for several cm).
- Not negligible noise (high input capacitance to the preamplifiers).

A further technological step: the CMOS VLSI approach

If the pixel size is small (below 100?m) and the number of pixels is large (above 1000) it is virtually impossible to bring the signal charge from the individual pixel to a chain of external read-out electronics even by using the advanced, fine-line, multi-layer, PCB technology.

When it is not possible to bring out the signal charge to external, peripheral electronics than it is the electronics that has to be brought in to the individual pixel!

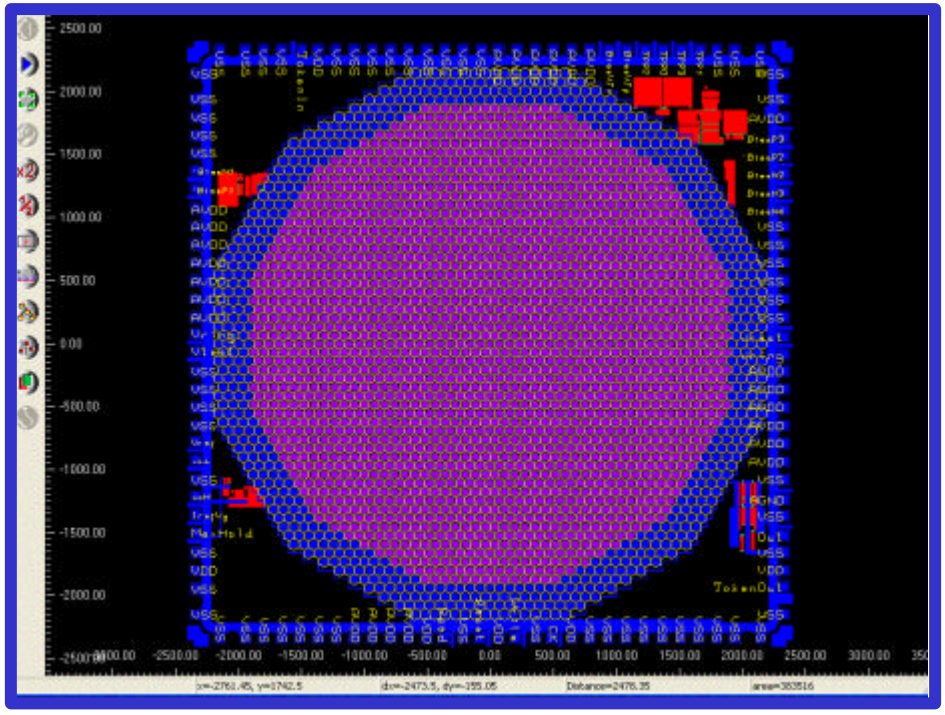

A CMOS full custom pixel array used directly as the charge collecting anode of the GEM has been designed, produced and it is currently under test.

Advantages: asynchronous, fast, low noise, honeycomb array design, no problems in the realization of the fan out to front-end electronics.

The collecting anode/read-out chip

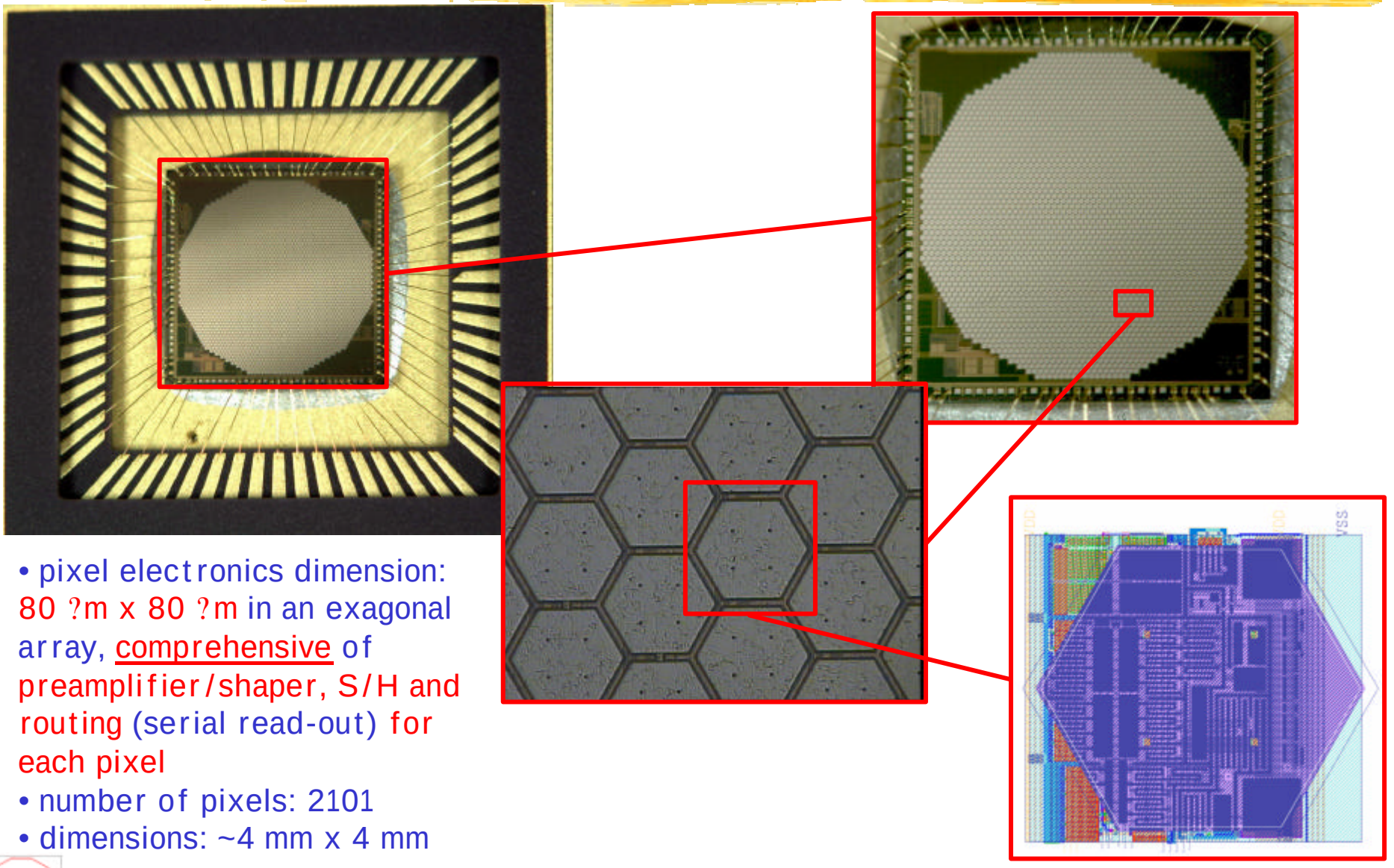

- pixel electronics dimension: 80 ?m x 80 ?m in an exagonal array, comprehensive of preamplifier/shaper, S/H and routing (serial read-out) for each pixel
- number of pixels: 2101
- dimensions: ~4 mm x 4 mm

PIXIE: the PIXel Imager Experiment

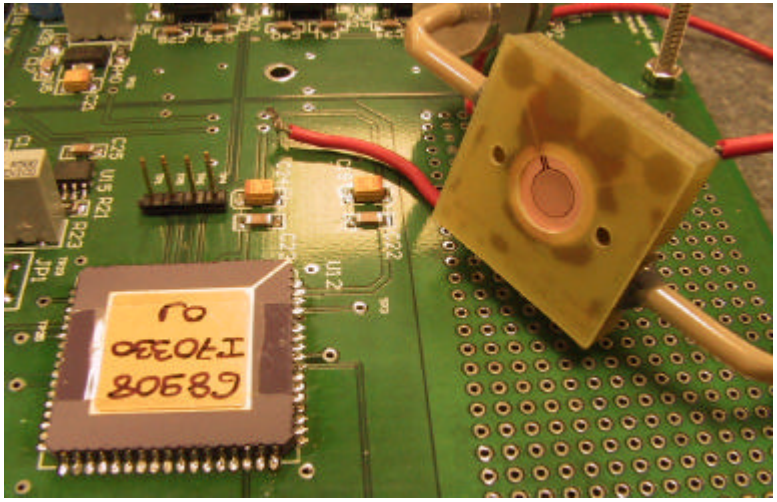

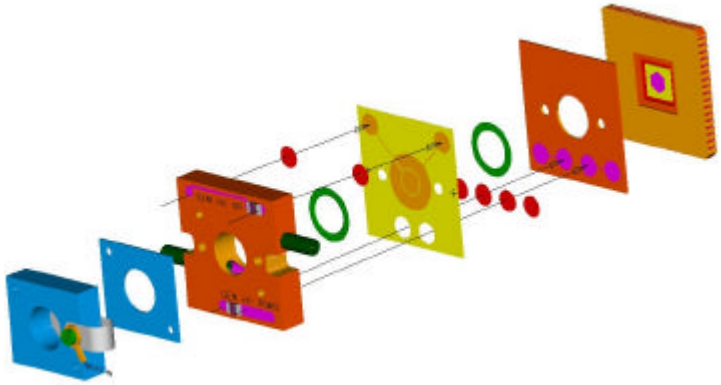

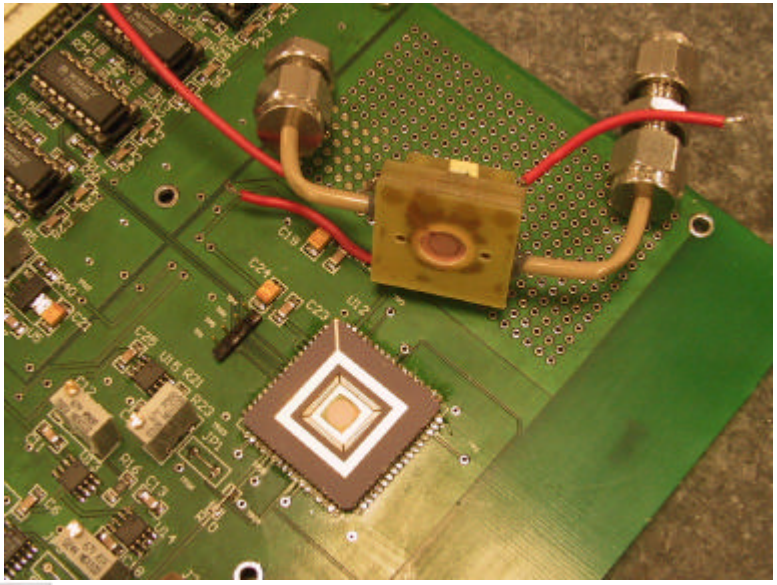

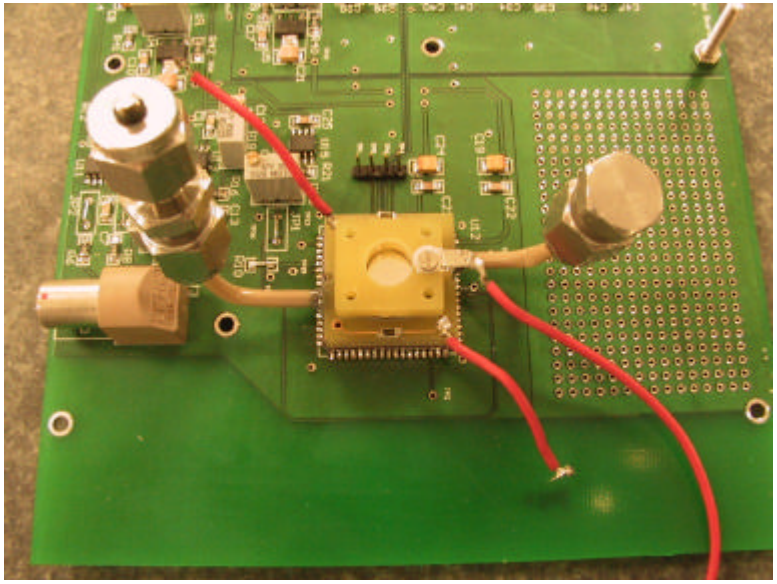

Detector and associated electronics are the same thing!

Electronics conceptual design

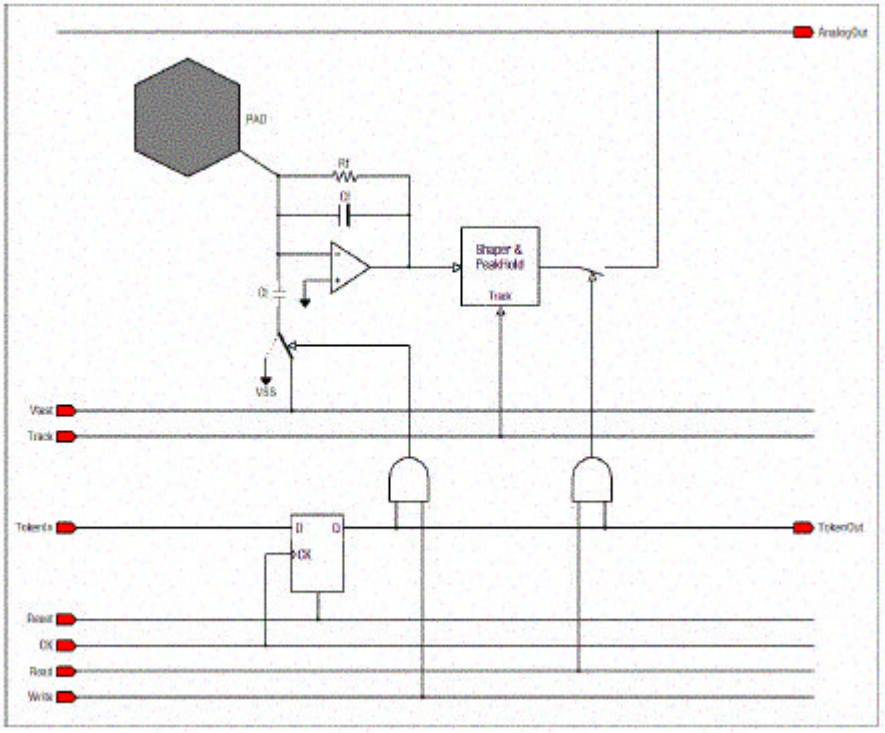

- ~3.5 microseconds shaping time
- 100 e^- ENC (very small detector capacitance)
- dynamic range: 0.2-20 fC
- power consumption: around 100 ?watt/pixel

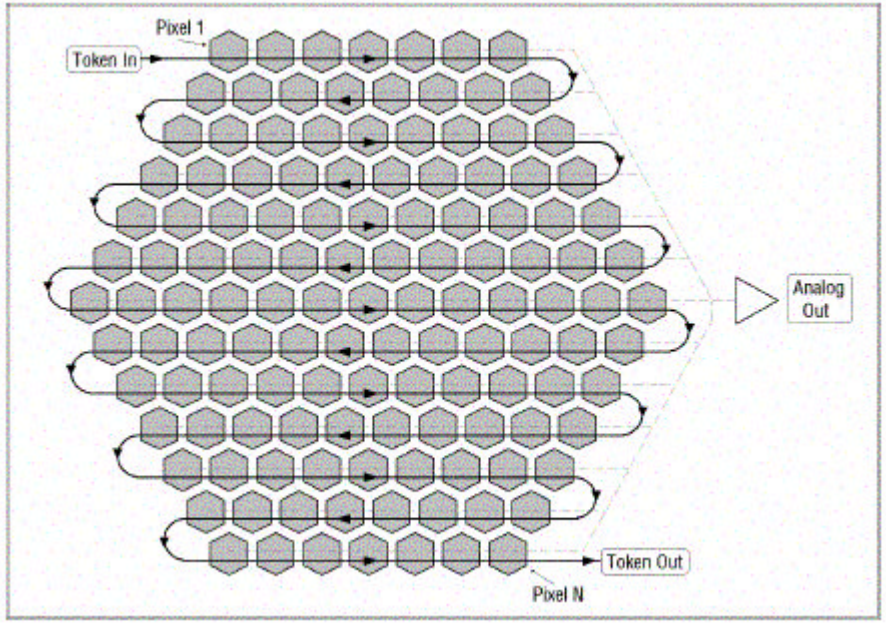

- external trigger (from the GEM) for parallel S/H on all the channels
- ADC after S/H: external , flash
- 400 ?s read-out time (with 5 MHz system clock)

Noise and gain measurement

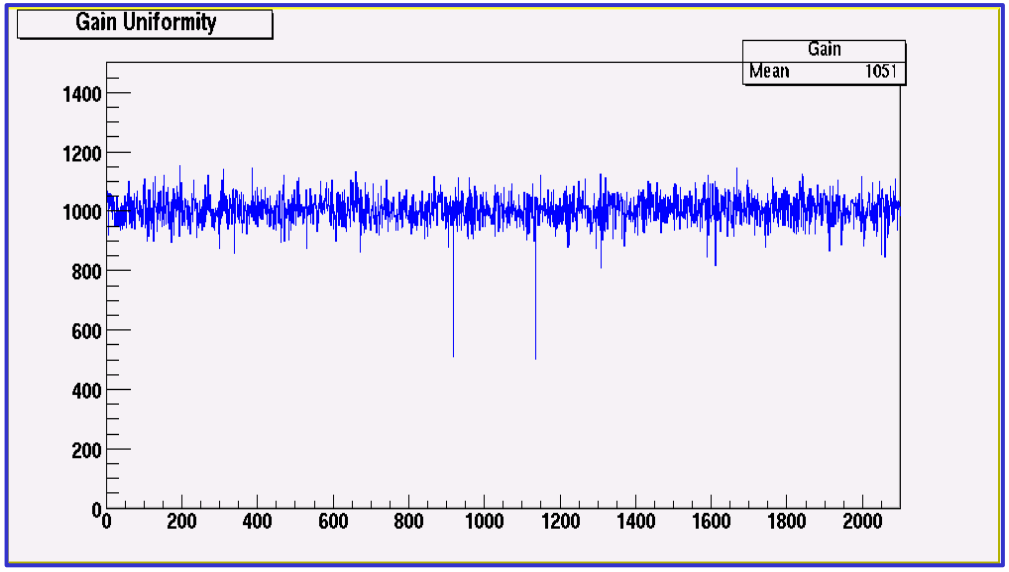

- Measured gain: ~ 100 mV/fC
- Gain uniformity across the channels: ~ 3% RMS

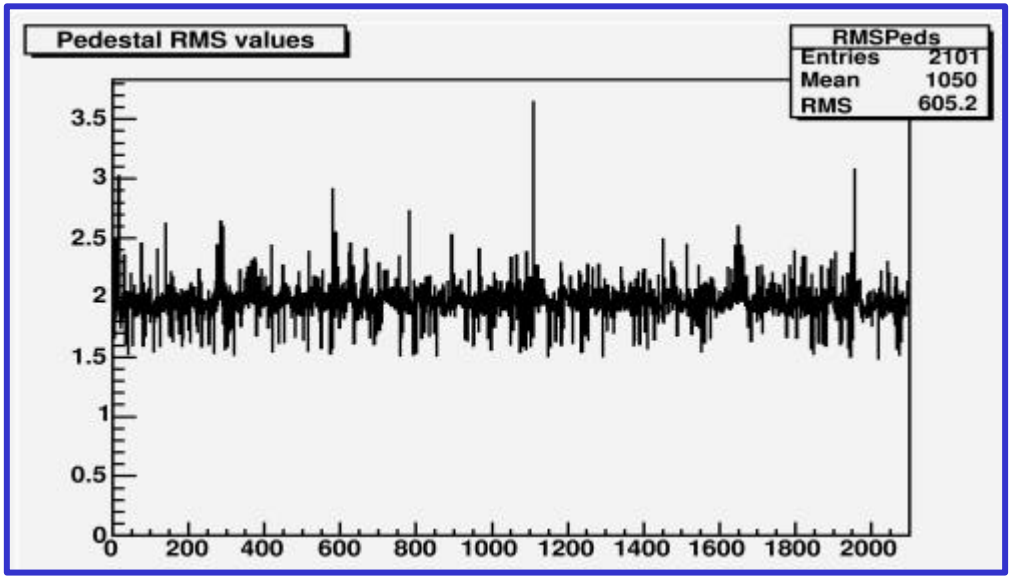

Noise RMS: ~ 100 e^- ENC (electronics gain is ~ 100 mV/fC): sensitive to the single primary electron with a gas gain < 1000 (easily achievable with a single GEM).

Internal calibration system and addressing capability

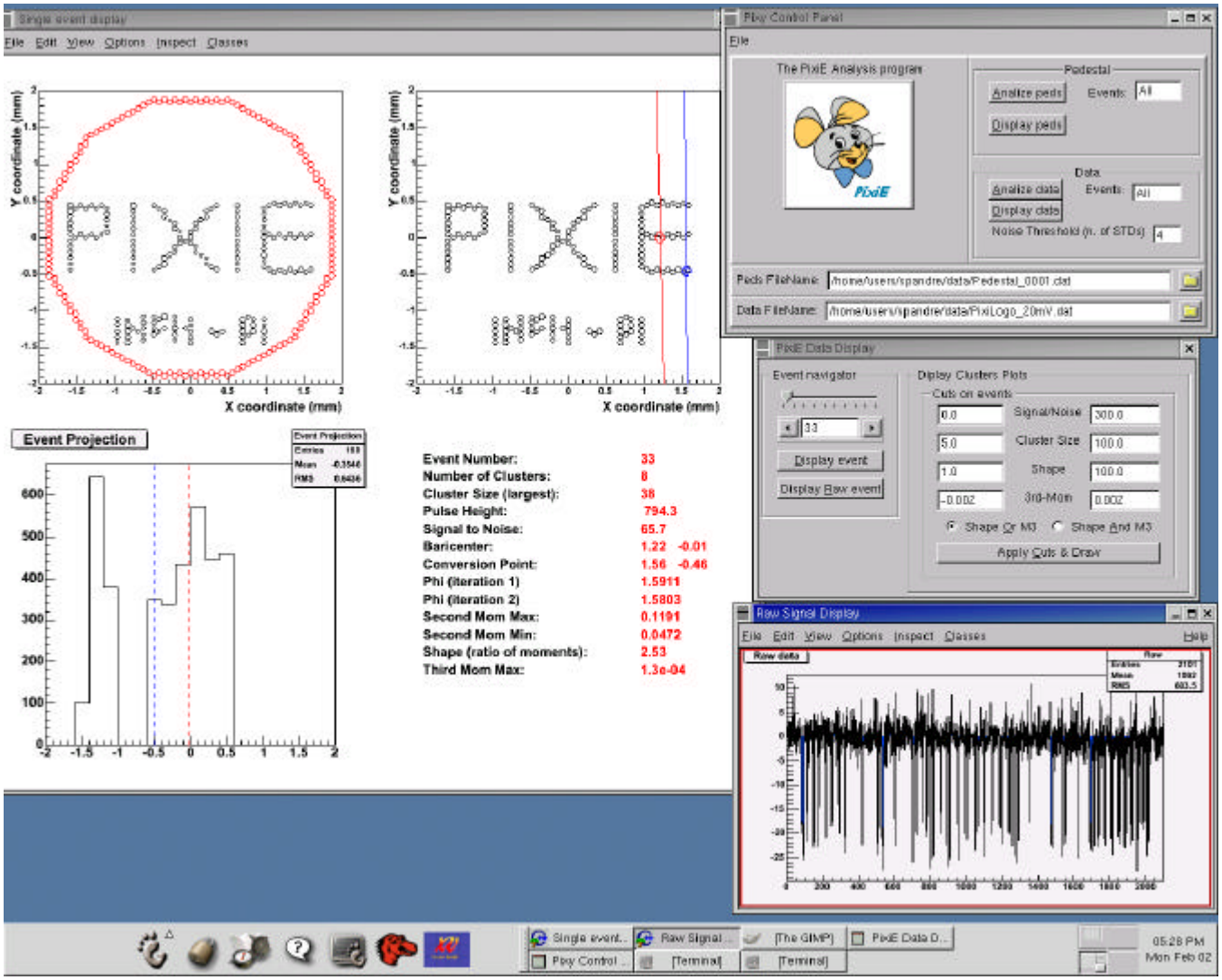

Detector response to 20 mV calibration signal (~1000 electrons) injected in a subset of pixels (carefully chosen).

Excellent response uniformity even before any attempt of calibration.

Some events…with 90 ?m pitch GEM

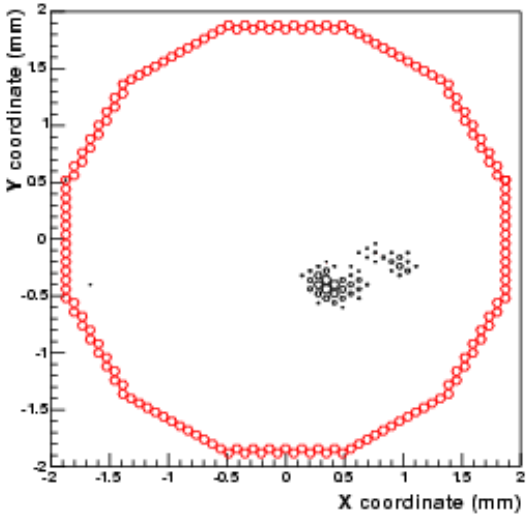

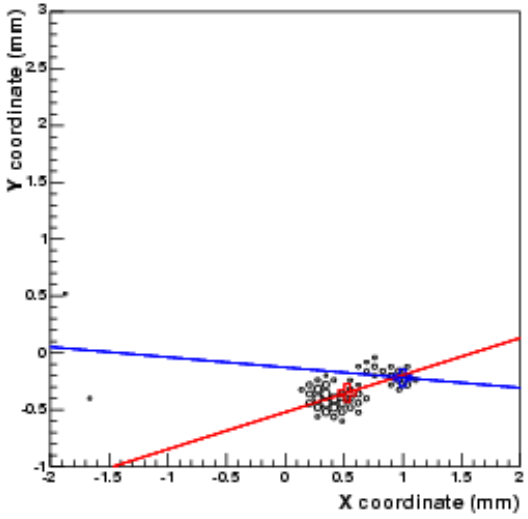

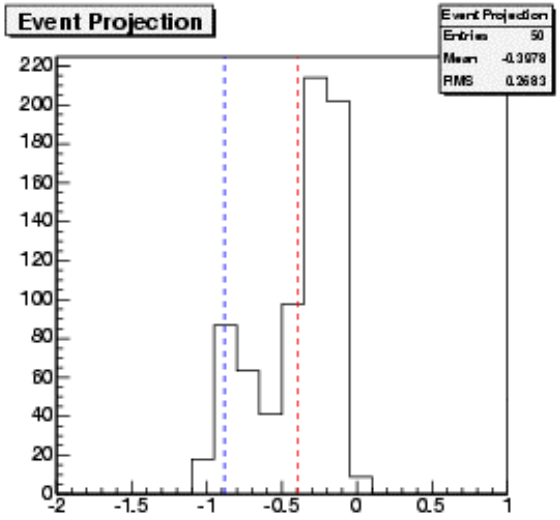

Event Number:	42
Number of Clusters:	3
Cluster Size (largest):	48
Pulse Height:	731.6
Signal to Noise:	51.0
Baricenter:	0.53 -0.35
Conversion Point:	1.00 -0.22
Phi (iteration 1)	-2.8264
Phi (iteration 2)	3.0521
Second Mom Max:	0.0720
Second Mom Min:	0.0098
Shape (ratio of moments):	7.31
Third Mom Max:	1.4e-02

Tracks “morphology”

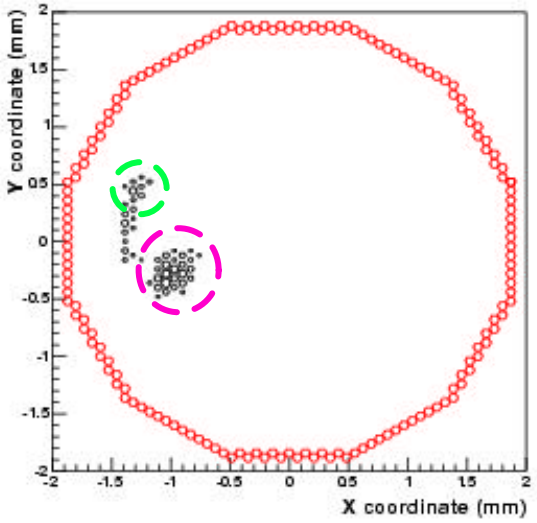

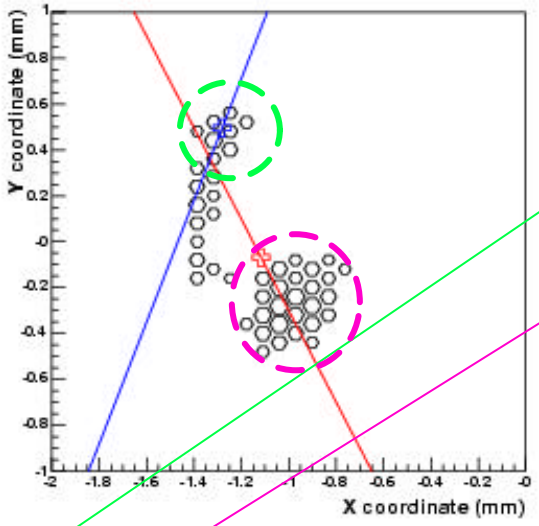

Auger Electron

Bragg Peak

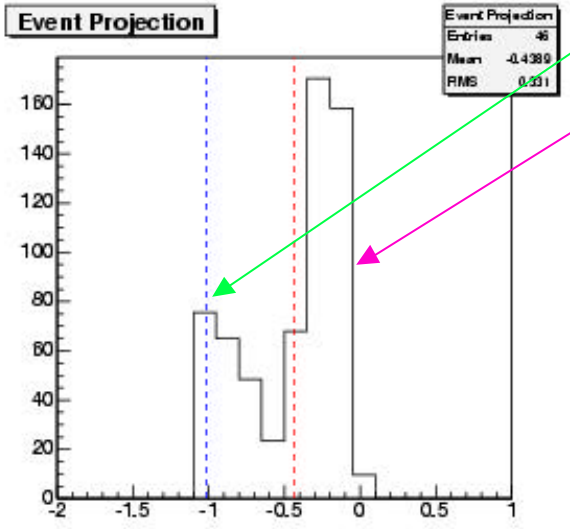

Event Number:	97
Number of Clusters:	1
Cluster Size (largest):	46
Pulse Height:	619.1
Signal to Noise:	45.4
Baricenter:	-1.12 -0.07
Conversion Point:	-1.28 0.49
Phi (iteration 1)	-1.1056
Phi (iteration 2)	-1.9310
Second Mom Max:	0.1095
Second Mom Min:	0.0168
Shape (ratio of moments):	6.51
Third Mom Max:	-2.3e-02

Raw data: less than 40000 electrons subdivided on 46 pixels!

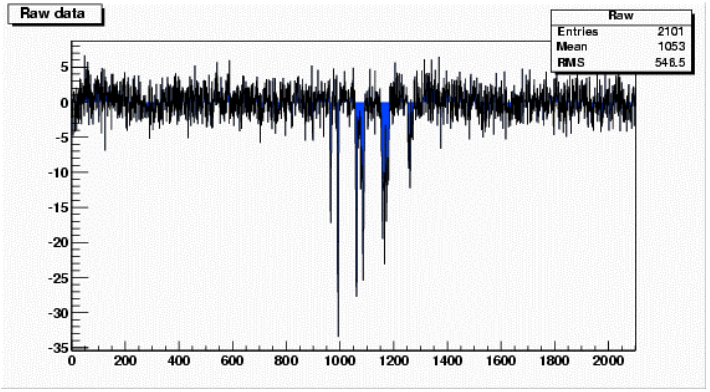

Tracks reconstruction

1) The track is recorded by the PIXel Imager

2) Baricenter evaluation

3) Reconstruction of the principal axis of the track: maximization of the second moment of charge distribution

4) Reconstruction of the conversion point: major second moment (track length) + third moment along the principal axis (asymmetry of charge release)

5) Reconstruction of emission direction: pixels are weighted according to the distance from conversion point.

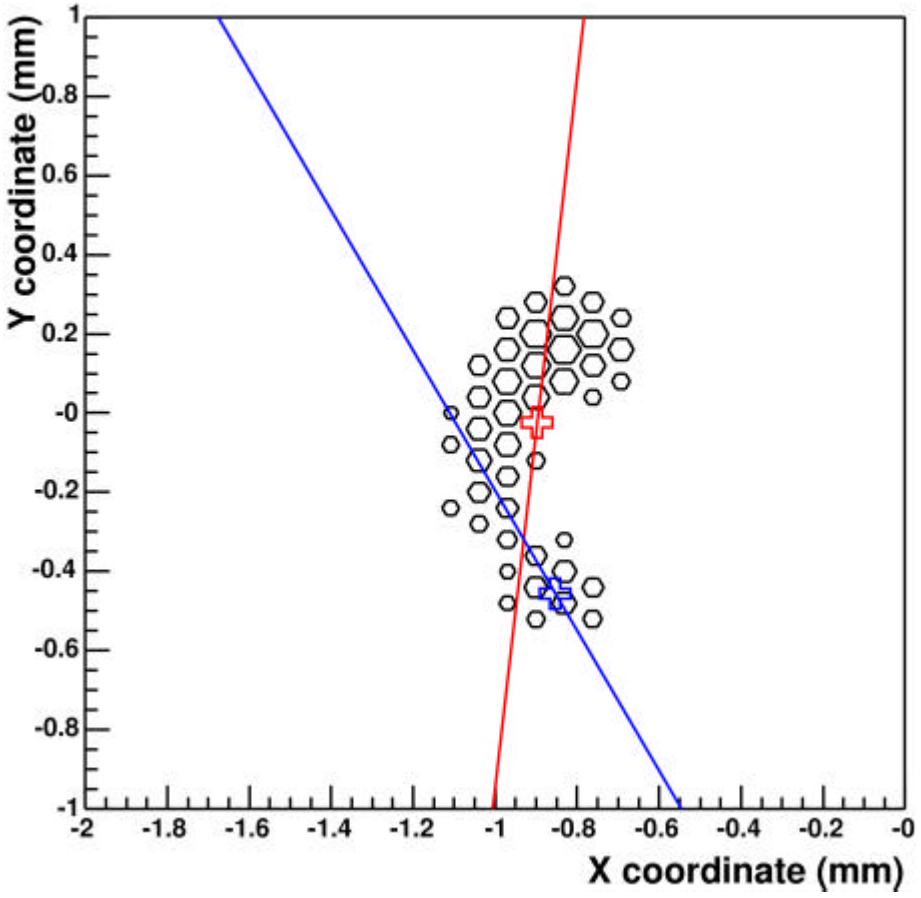

A new 50 ?m pitch GEM

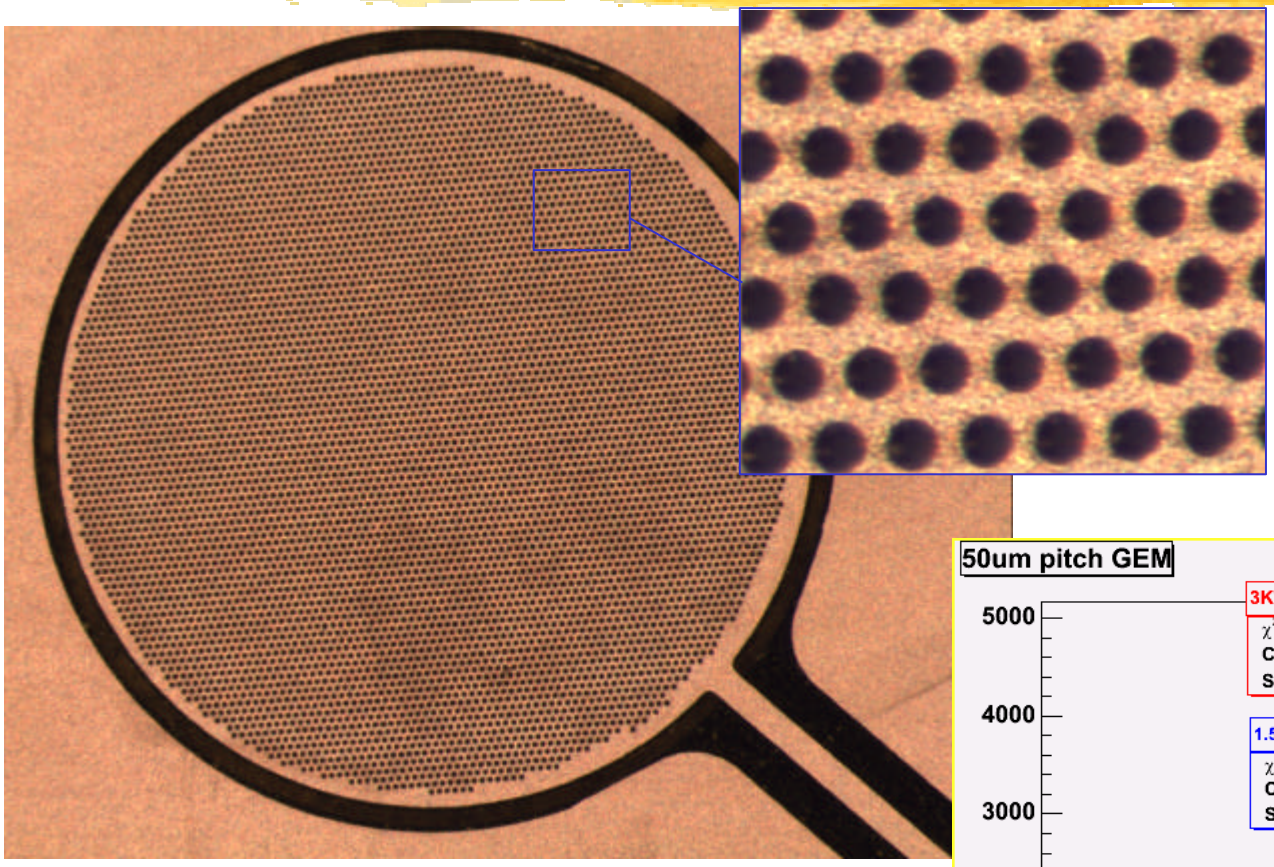

pitch – 50 ?m

? hole – 30 ?m

thickness – 25 ?m

Effective Gain ~ Gain · ?collection

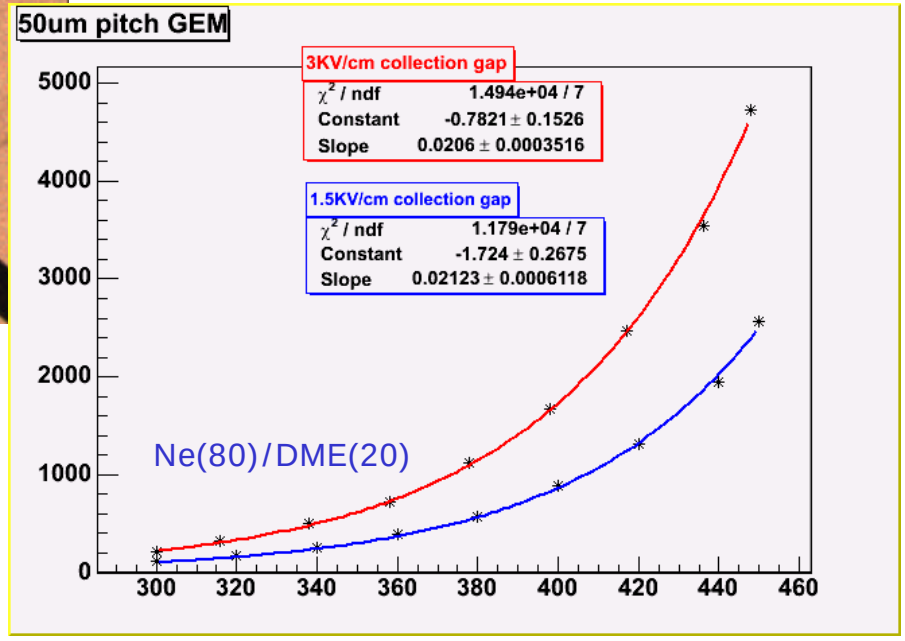

First events with the 50 ?m pitch GEM

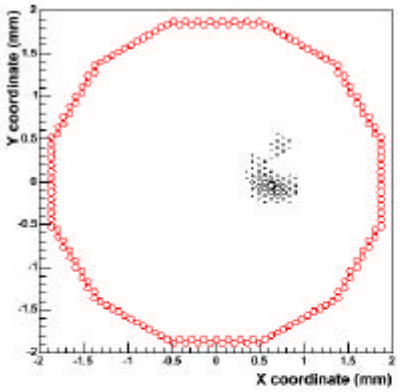

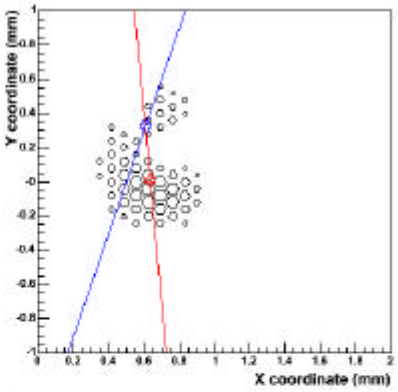

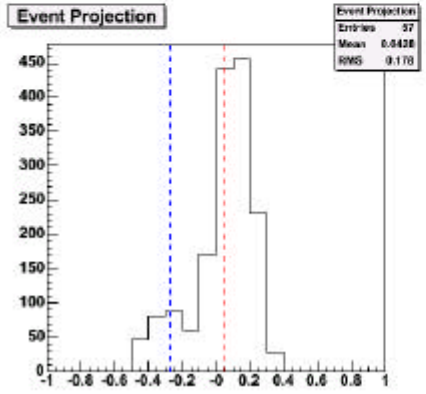

Event Number:	21
Number of Clusters:	1
Cluster Size (largest):	57
Pulse Height:	1603.1
Signal to Noise:	107.2
Baricenter:	0.64 0.01
Conversion Point:	0.61 0.33
Phi (iteration 1)	-1.4802
Phi (iteration 2)	-1.8908
Second Mom Max:	0.0317
Second Mom Min:	0.0173
Shape (ratio of moments):	1.83
Third Mom Max:	-6.2e-03

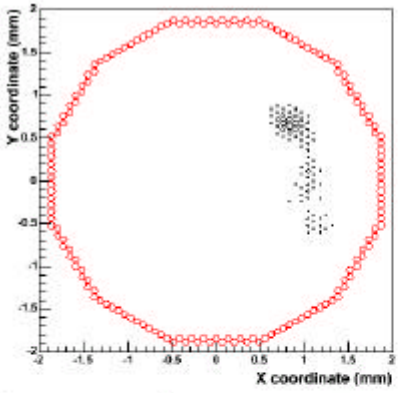

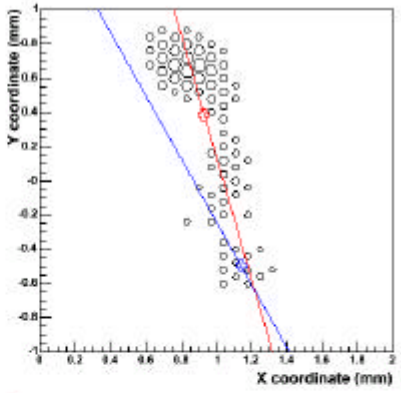

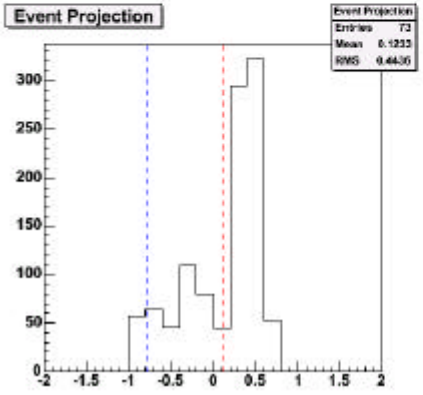

Event Number:	10
Number of Clusters:	1
Cluster Size (largest):	73
Pulse Height:	1070.4
Signal to Noise:	63.2
Baricenter:	0.93 0.39
Conversion Point:	1.14 -0.50
Phi (iteration 1)	1.8431
Phi (iteration 2)	2.0696
Second Mom Max:	0.1968
Second Mom Min:	0.0109
Shape (ratio of moments):	18.00
Third Mom Max:	8.0e-02

Full detector simulation

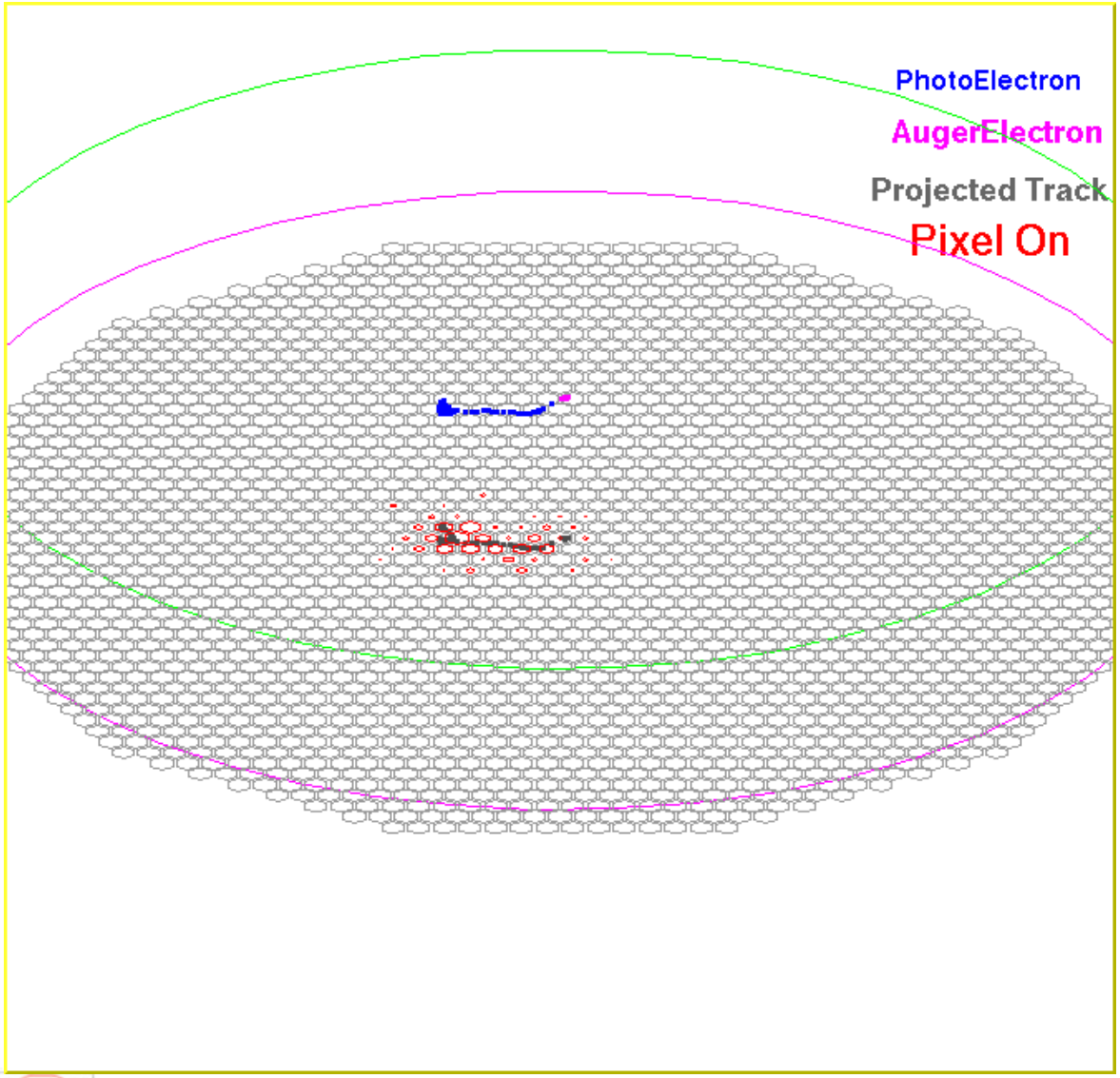

- Generation (photoelectron + Auger)
- Propagation (SS_MOTT)
- Creation and diffusion of primary ionization (Maxwell, Garfield, Magboltz)
- Gas multiplication
- Digitization
- Pixel Representation

Polarimetric sensitivity: modulation factor

Modulation factor as a function of the energy for different mixtures

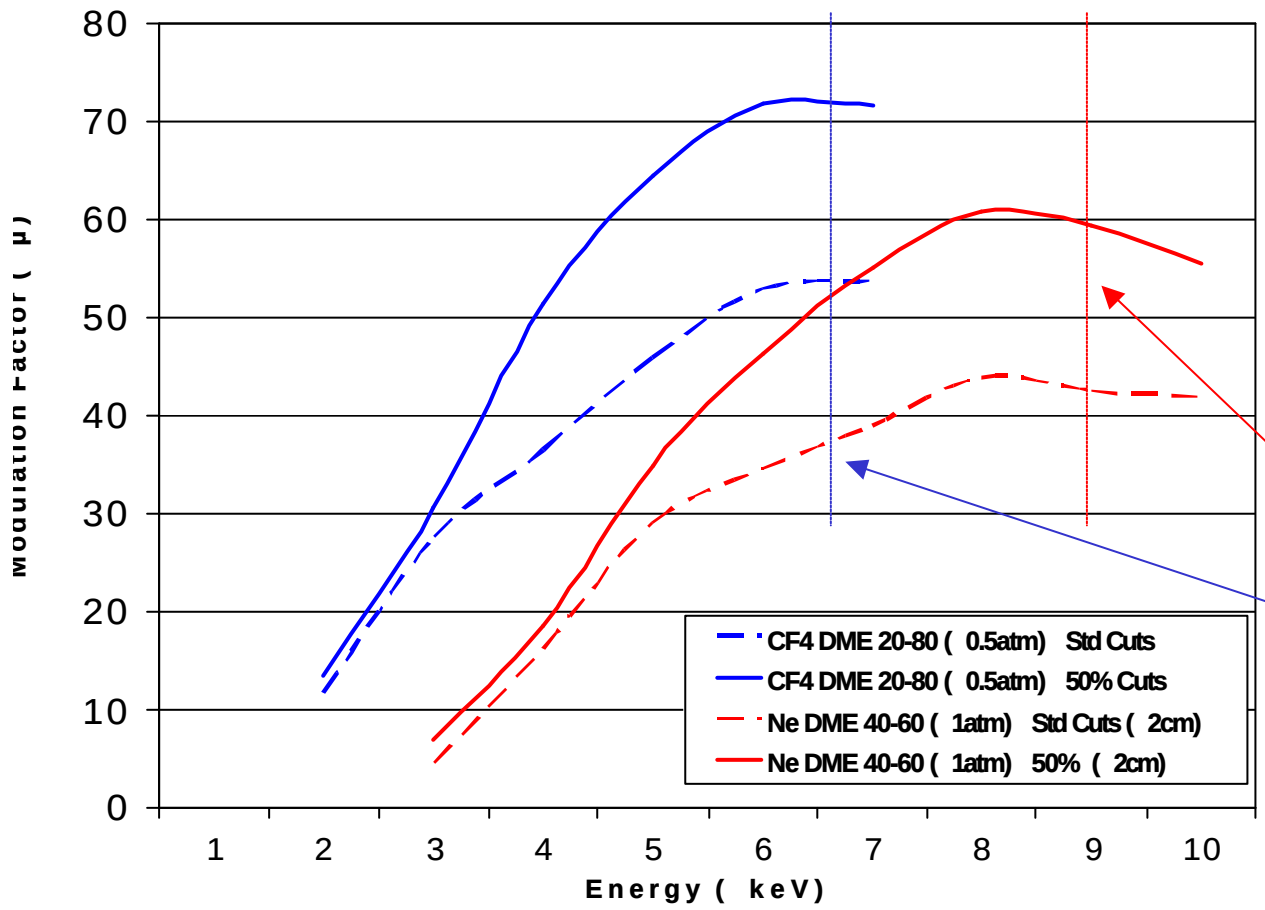

Std cuts = all the events
50% cuts = selection on the "shape" of the tracks preserving 50% of the events.

Two possible different gas mixtures for two energy ranges

Reconstruction algorithm to be refined at high energies

Polarimetric sensitivity: MDP

MDP for strong sources (Crab and Her-X1) with different gas mixtures and different pressures, 1000 cm^2 mirror collecting area.

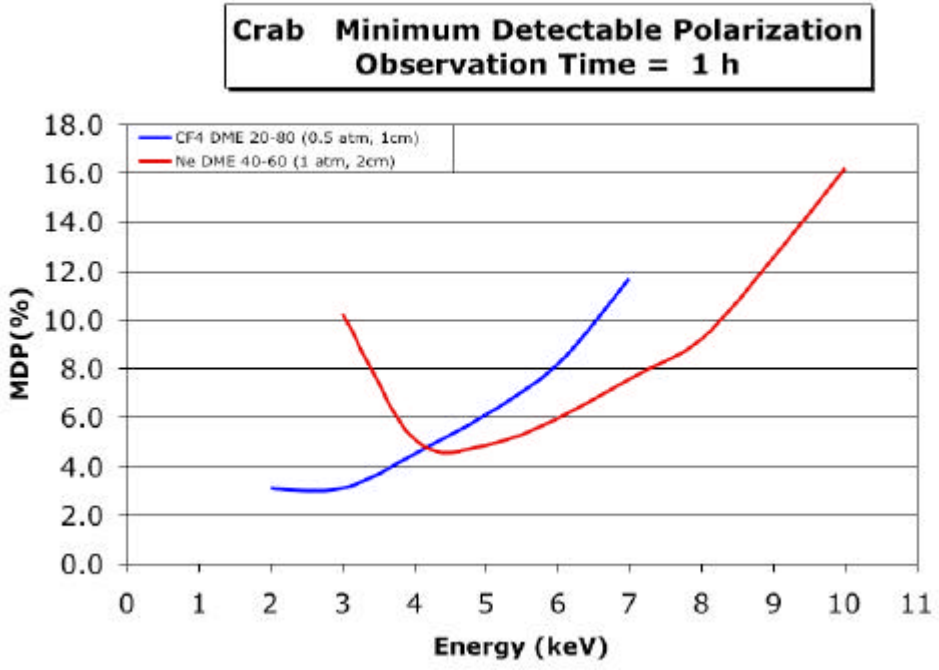

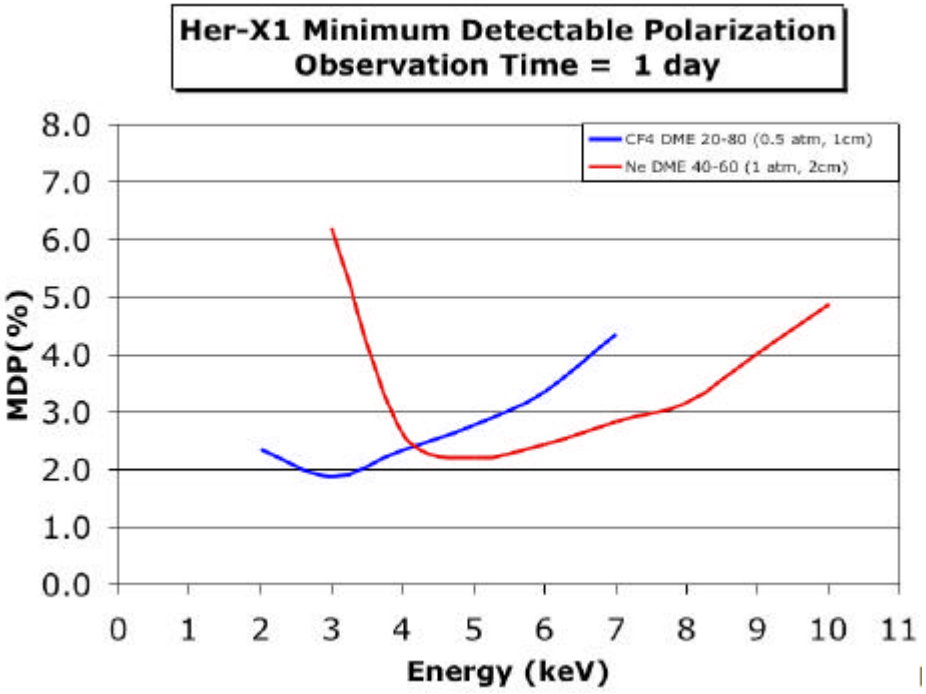

MDP(3?): CRAB

CF4/DME, good at low energy ~ 2.1 %

Ne/DME, 2cm, good at high energy ~ 3.5 %

MDP(3?): Her-X1 (~ 100 mCrab)

CF4/DME, good at low energy ~ 1.2 %

Ne/DME, 2cm, good at high energy ~ 1.4 %

What matters ? The transverse diffusion…

6 keV polarized photons in CF4-DME 20-80, 0.5atm-like mixture
(**same events, same gas properties with different diffusion coefficients**)

$? ? \frac{120?m}{\sqrt{cm}}$

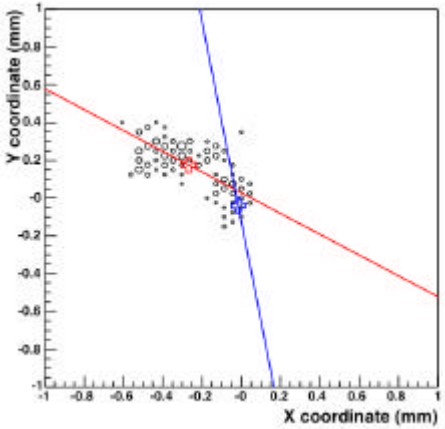

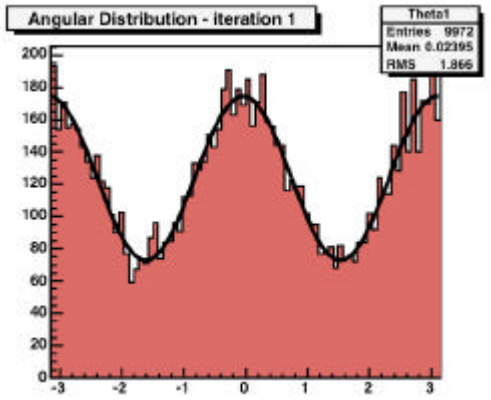

? ? 41%

$? ? \frac{60?m}{\sqrt{cm}}$

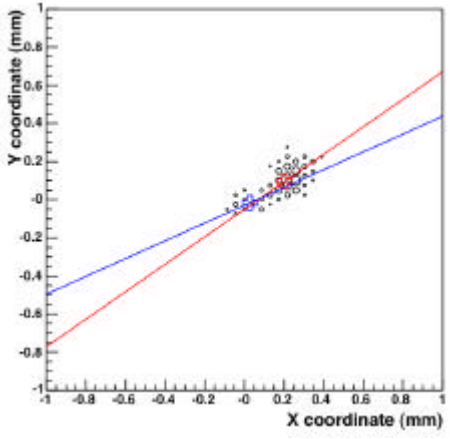

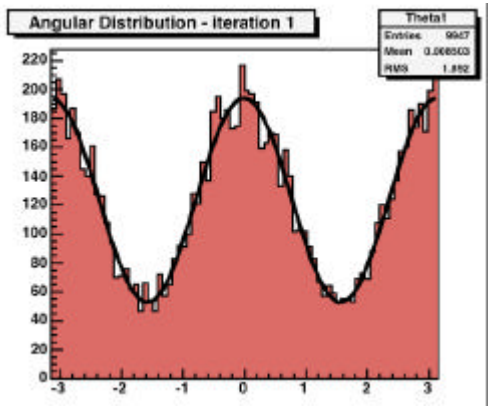

? ? 57%

Transverse diffusion scale as 1/vP :
High pressure -> Low diffusion , short tracks
Low pressure -> Long tracks , high diffusion

What matters ? The Read-out sampling

2 keV polarized photons in CF4-DME 20-80, 0.5atm
(same events, with different pixel pitch)

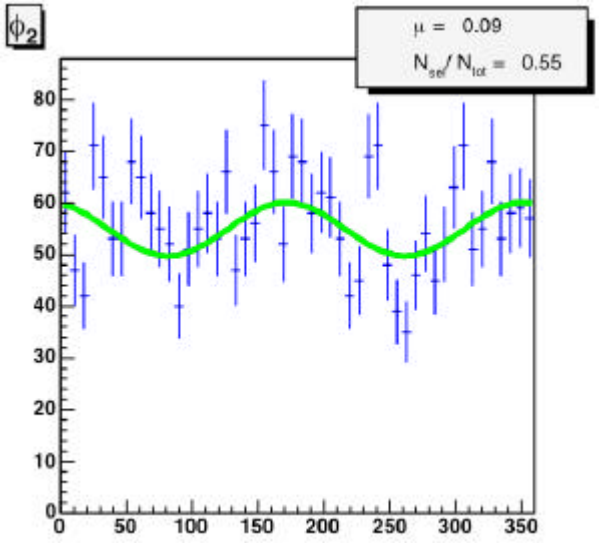

pitch ? 80?*m*
? ? 9%

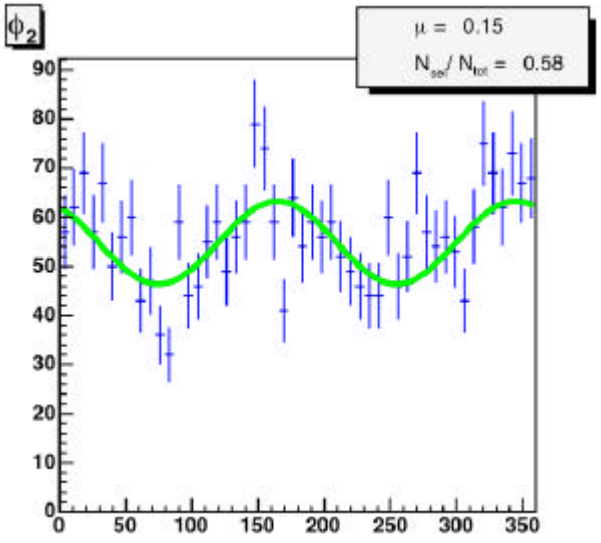

pitch ? 50?*m*
? ? 15%

The pixel pitch size is critical at low energies!

Hexagonal vs Square Readout

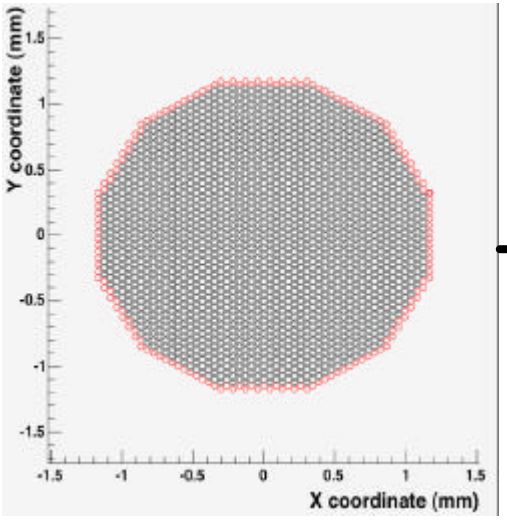

Hexagonal pixel map with 50μm pitch

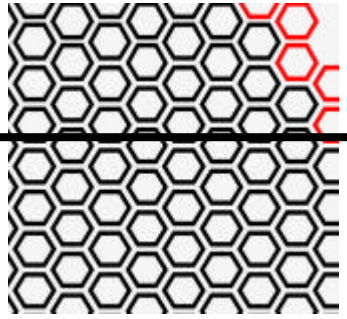

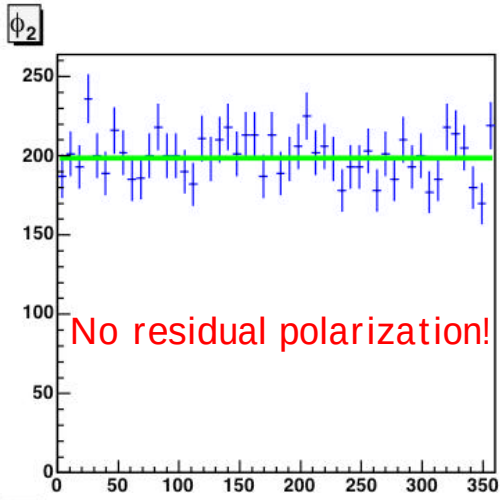

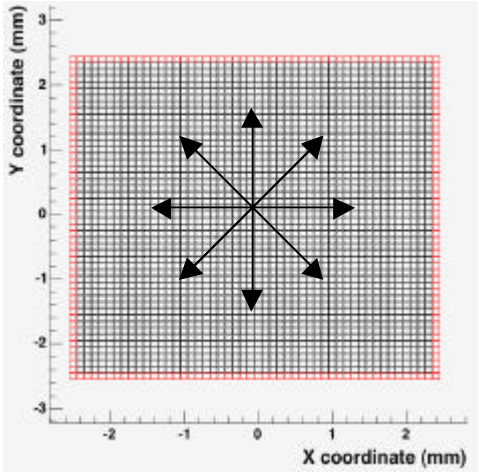

Square pixel map with 100μm pitch

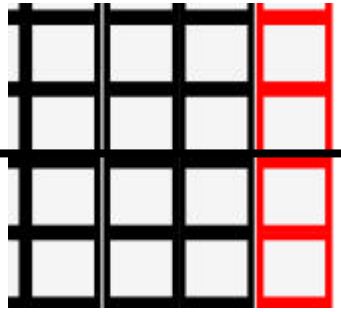

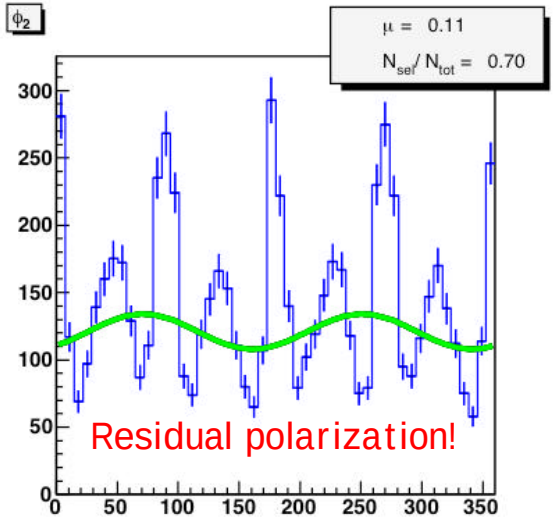

Unpolarized Run, 2 keV CF4/DME 20-80 0.5 atm

Future perspectives: new chip implementation

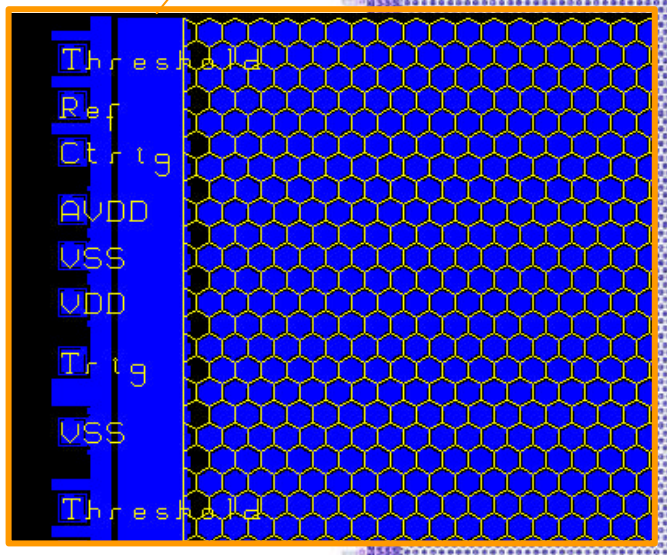

Square matrix of maximum area :12x12 mm^2
Active area : 11x11 mm^2
8 sectors of 2.8k hexagonal pixels each
80 ?m pitch
8 parallel analog buses
10 MHz read-out frequency
280 ms (read-out time) frame rate
1 kHz source rate possible

clock drivers, bias circuitry, trigger output & analog buffer placed on the left- and right-hand sides

Submitted: 1st May
Delivery: beginning of June

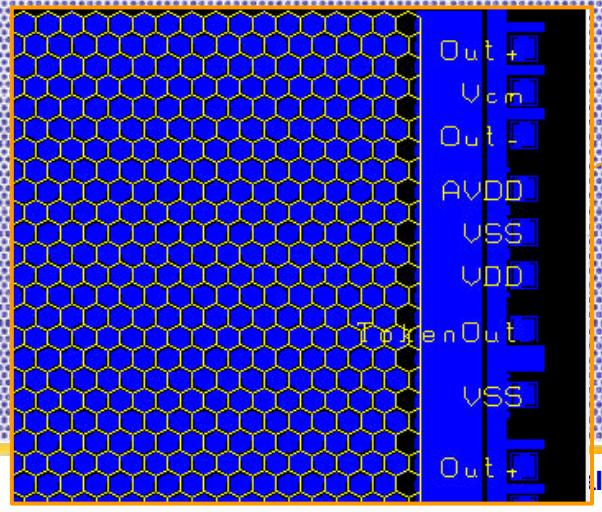

Summary: key features of the PIXel Imager

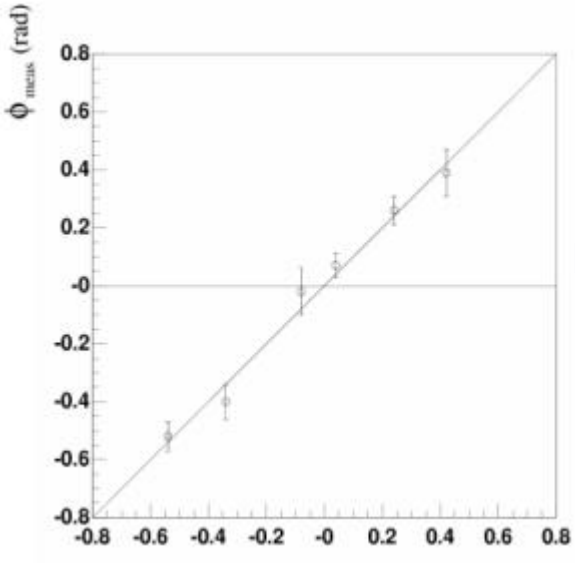

Angular linearity

Polarimetry

(Up to50 -70 % modulation factor, broad-band, not dispersive, does not require rotation, large Signal/Background ratio – thanks to the small dimensions)

+

Imaging

(~50 ?m spatial resolution, truly 2-D)

+

Spectroscopy

(~ 15% FWHM @ 6 keV, at the level of a good proportional counter)

+

Timing

(few ns time resolution - given by the GEM, read with fast electronics – less than 1 ms dead time)

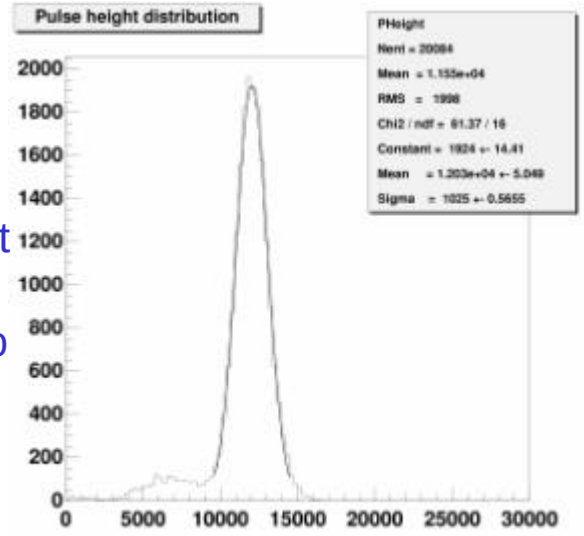

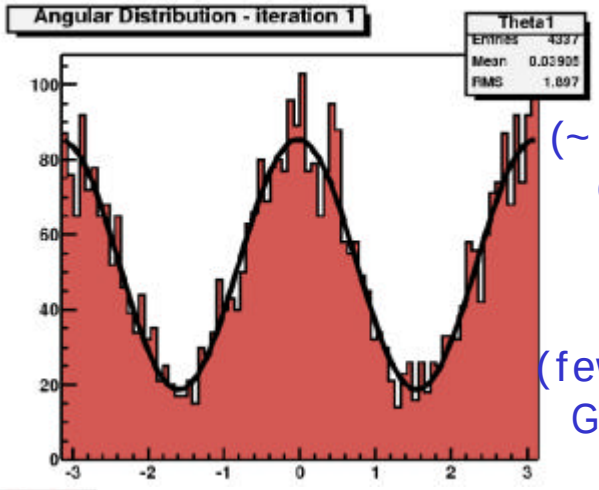

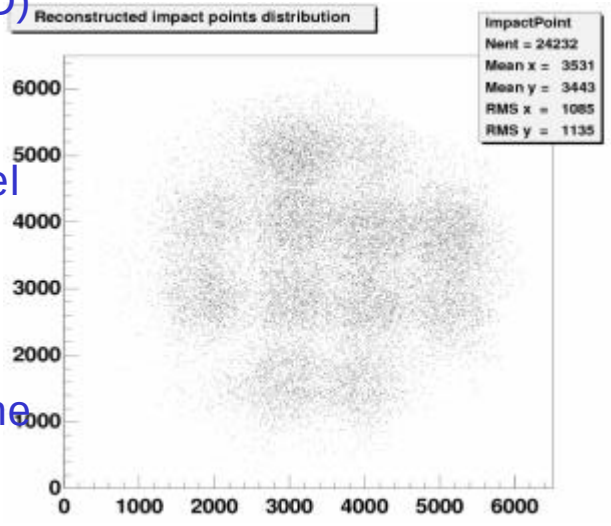

Conclusions

A system in which the GEM foil, the absorption gap and the entrance window are assembled directly over a CMOS chip die has been developed. The ASIC itself becomes at the same time, the charge collecting anode and the pixelized read-out of a MicroPattern Gas Detector. The full electronics chain and the detector are completely integrated.
At a gain of 1000 a high sensitivity to single primary electron detection is reached. No problems found up to now in operating the system under HV and in gas environment.
Final design will have 16-32 k channels and 60-70 microns pixel size. This would open new directions in gas detector read-out, bringing the field to the same level of integration of solid state detectors.

The performance of the tested prototypes looks like a significant step forward, compared with traditional X-ray polarimeters and promises a large increase in sensitivity. Observations will measure energy fluxes and polarization of the flux as functions of time/energy and will image the source.
In its final configuration the MPGD target performance is the detection of ~few% polarization for few mCrabs sources (in the XEUS focal plane, for example). This sensitivity will likely allow polarimetry measurements to be made on thousands of galactic and extragalactic sources: a real breakthrough in X-ray astronomy.

EXTRAS...

The choice of gas mixture

Leading criteria in the choice of the gas mixture:

- Low K-edge (low Z materials)
- Low electromagnetic scattering, favorable slowing down/scattering ratio (low Z materials)
- Favorable range/pixel size ratio
- High detection efficiency (high Z materials)
- Small tranverse diffusion in the charge drift (organic quenchers)

Mixture	Min. Diff. (µm/cm^1/2)	Efficiency (1cm) @ 6 keV	Efficiency (1cm) @ 2 keV	Electron Range @ 6 keV (um)	Electron Range @ 2 keV (um)
Ne/DME 80/20, 1atm	132	5.42%	71.63%	1004	188
Ne/DME 50/50, 1atm	85	5.15%	70.71%	768	144
Ne/DME 40/60, 1atm	77	5.06%	70.41%	712	133
Ne/DME 20/80, 1atm	67	4.33%	65.68%	622	116
CF4/DME 20/80, 1 atm	57	4.73%	70.34%	467	87
CF4/DME 20/80, 0.5 atm	81	2.39%	45.55%	934	175
CF4/DME 20/80, 0.25 atm	120	1.20%	26.19%	1870	350
DME, 1 atm	61	3.00%	55.90%	552	103
DME, 0.5 atm	86	1.50%	33.60%	1104	207
Propane, 1 atm	136	1.80%	39.29%	577	108
Propane, 0.5 atm	192	0.90%	22.09%	1154	216
Propane, 2 atm	96	3.56%	63.14%	288	54

Monte Carlo simulation: propagation of the photoelectron

Photoelectron transport code originally developed by D. Joy for electron microscopy (particularly accurate at low energies) - adapted for the transport in gas mixtures.

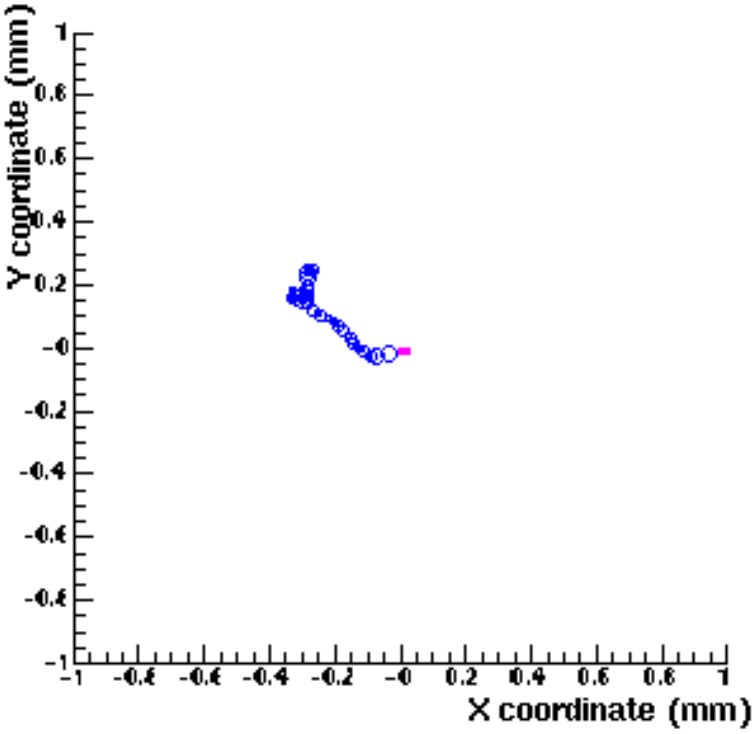

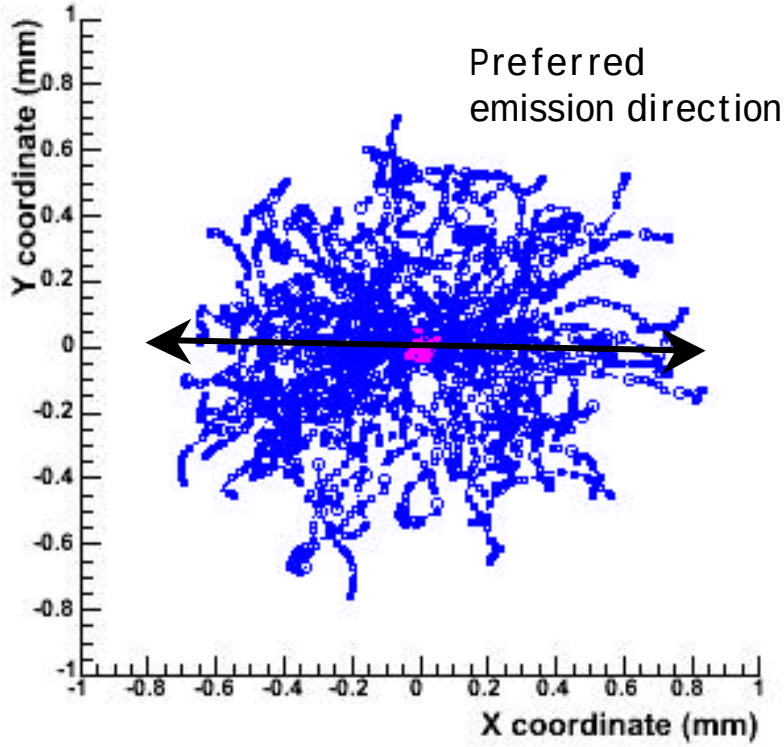

Photoelectron and Auger propagation in Ne/DME 80/20

Basics of photoelectric effect in gas III

5.0 keV photoelectrons tracks in Ne (100% linearly polarized, collimated photons beam).

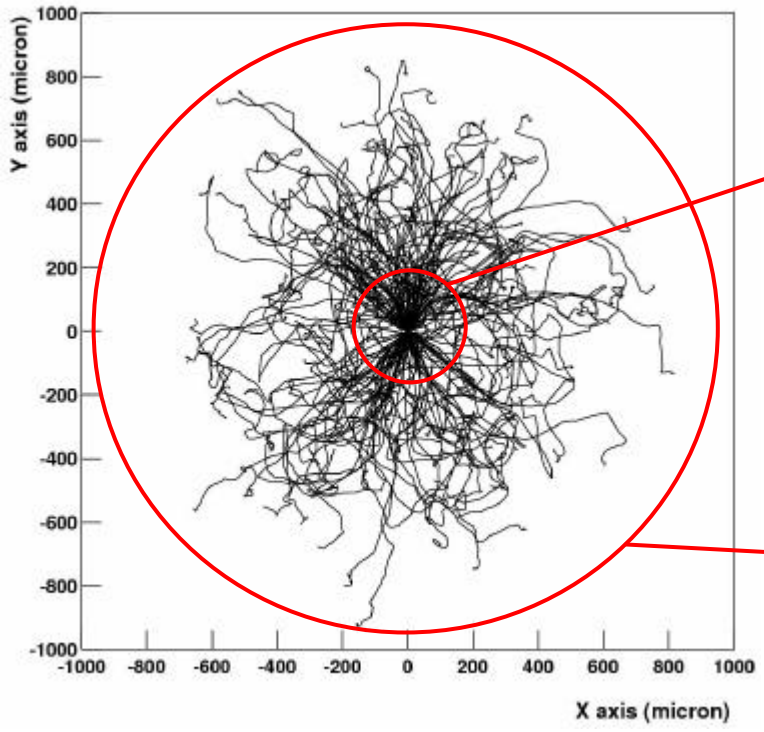

Modulation factor, as evaluated from charge released within a certain distance from conversion point.

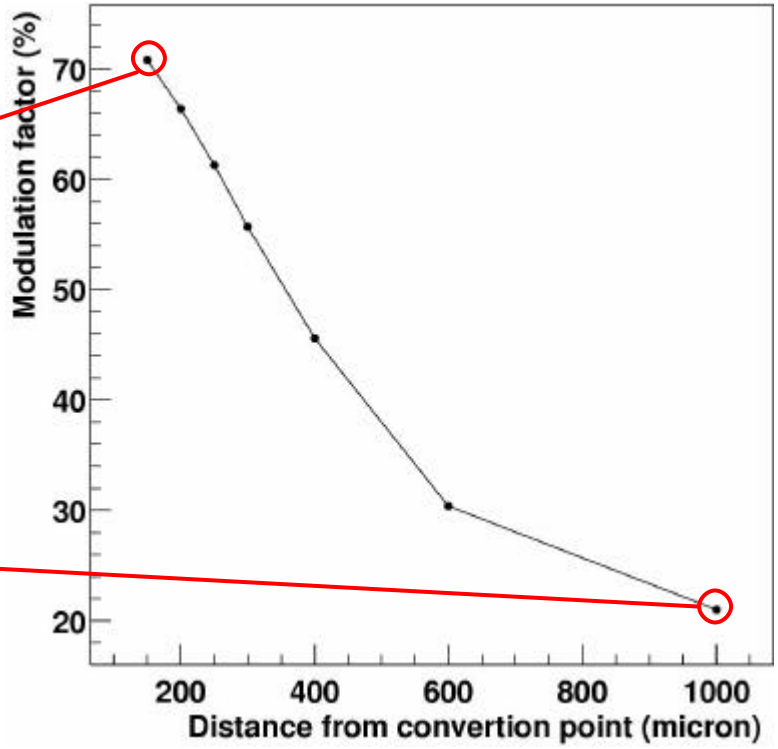

MC simulation: electric field and electron transport in gas

Cell geometry, materials, boundary conditions

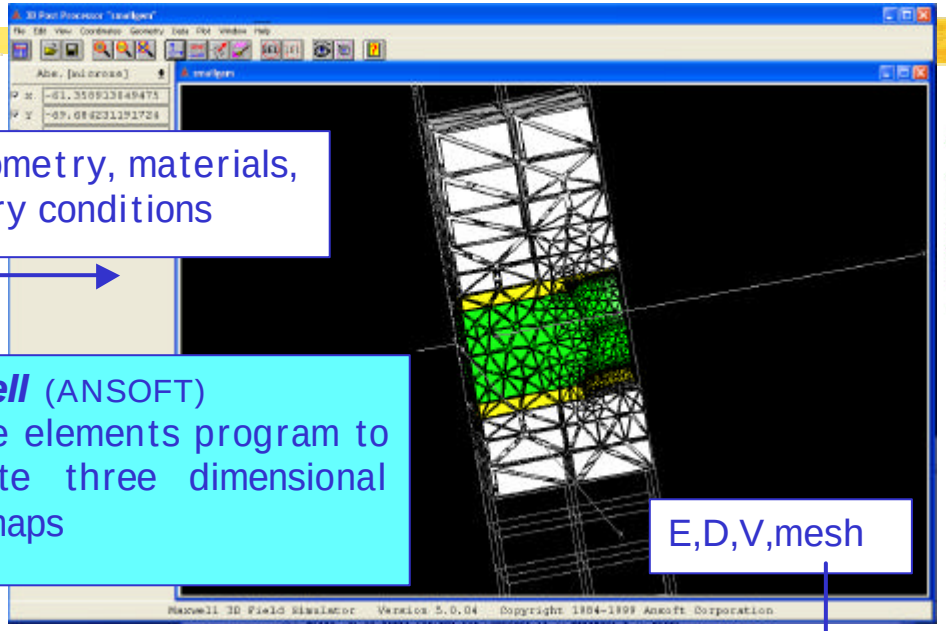

Maxwell (ANSOFT)
a finite elements program to compute three dimensional field maps

E,D,V,mesh

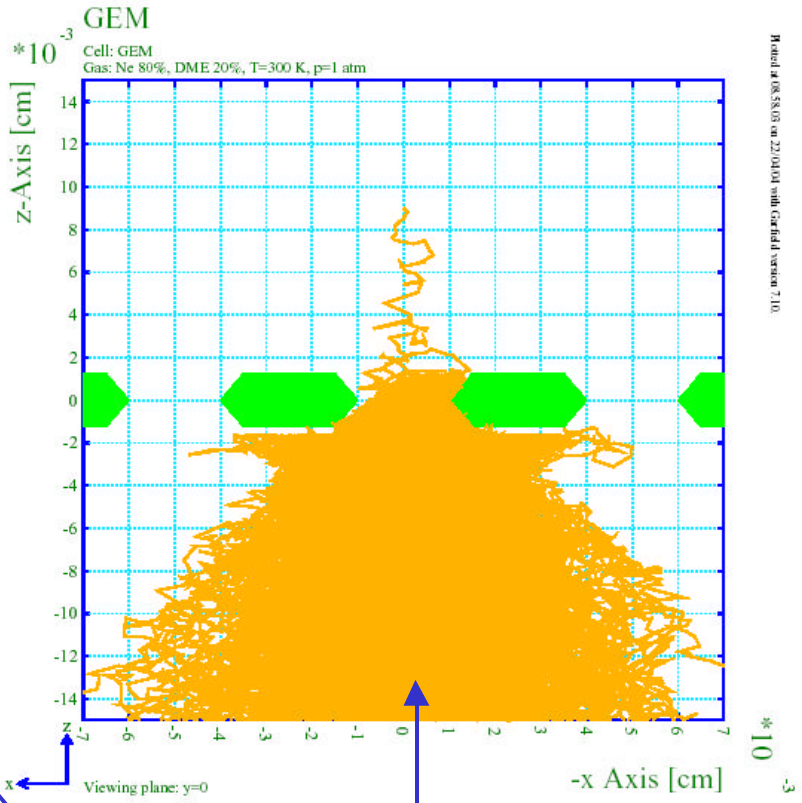

Gas mixture

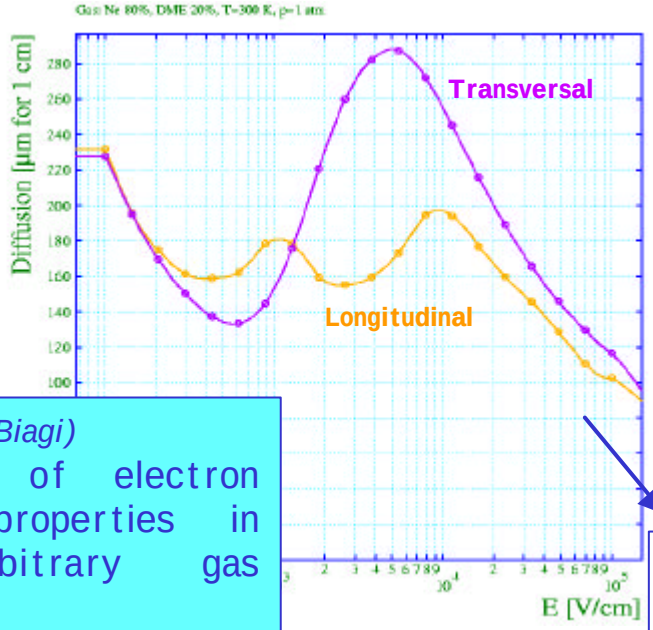

Magboltz *(S.Biagi)*
computation of electron transport properties in nearly arbitrary gas mixtures

Garfield *(R. Veehnof)*
MC 3D-simulation of drifting particles, including diffusion and avalanches generation

drift, diffusion, gain and attachment of electrons/ions vs E

The analog signal

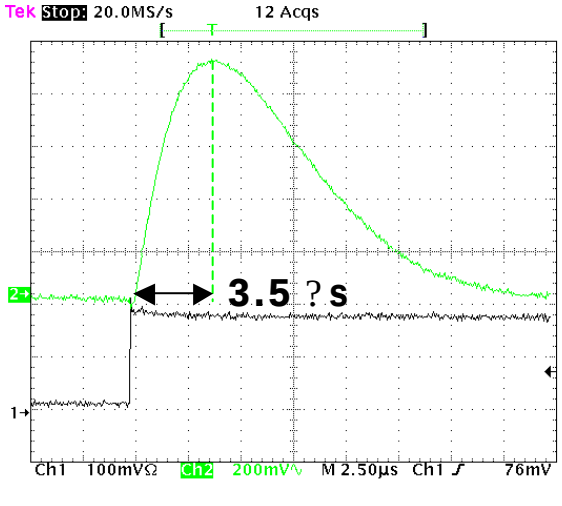

Analog output
(60000 electrons)

Write signal
(no Maxhold)

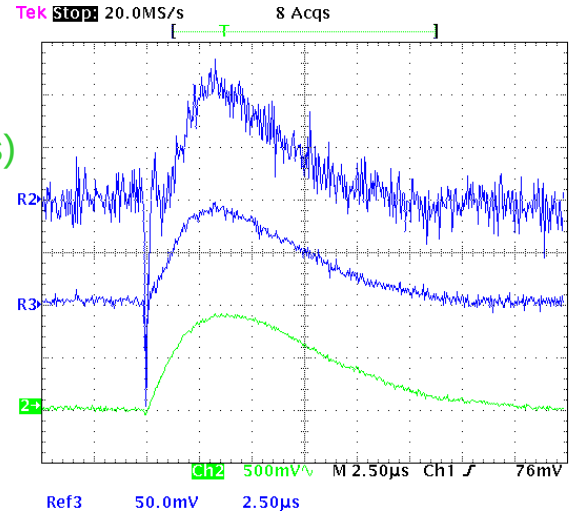

Analog output
(1000 electrons)

Analog output
(6000 electrons)

Analog output
(60000 electrons)

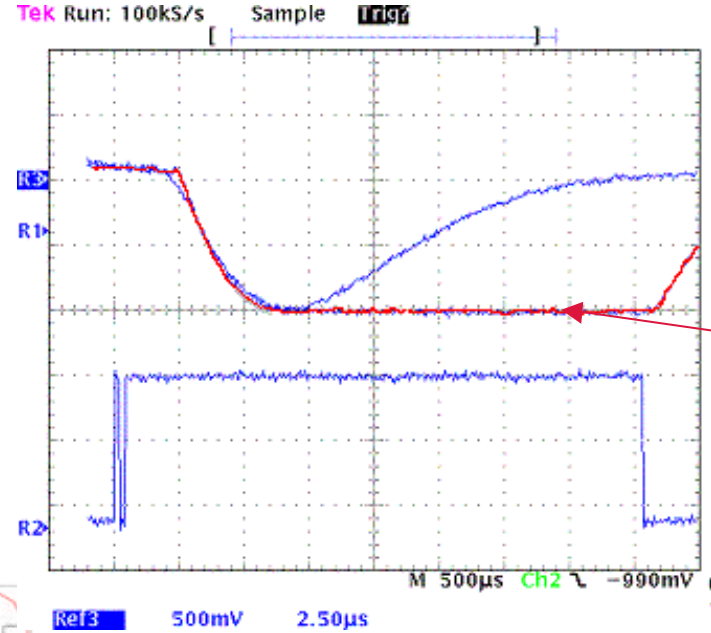

Shaper output

S/H analog output

Maxhold signal

Automatic search of the maximum of the signal within a 10 ?sec window after an asyncronous external trigger (from the TOP GEM)

Angular reconstruction

Theoretical Emission Direction

Basic algorithm

Second iteration

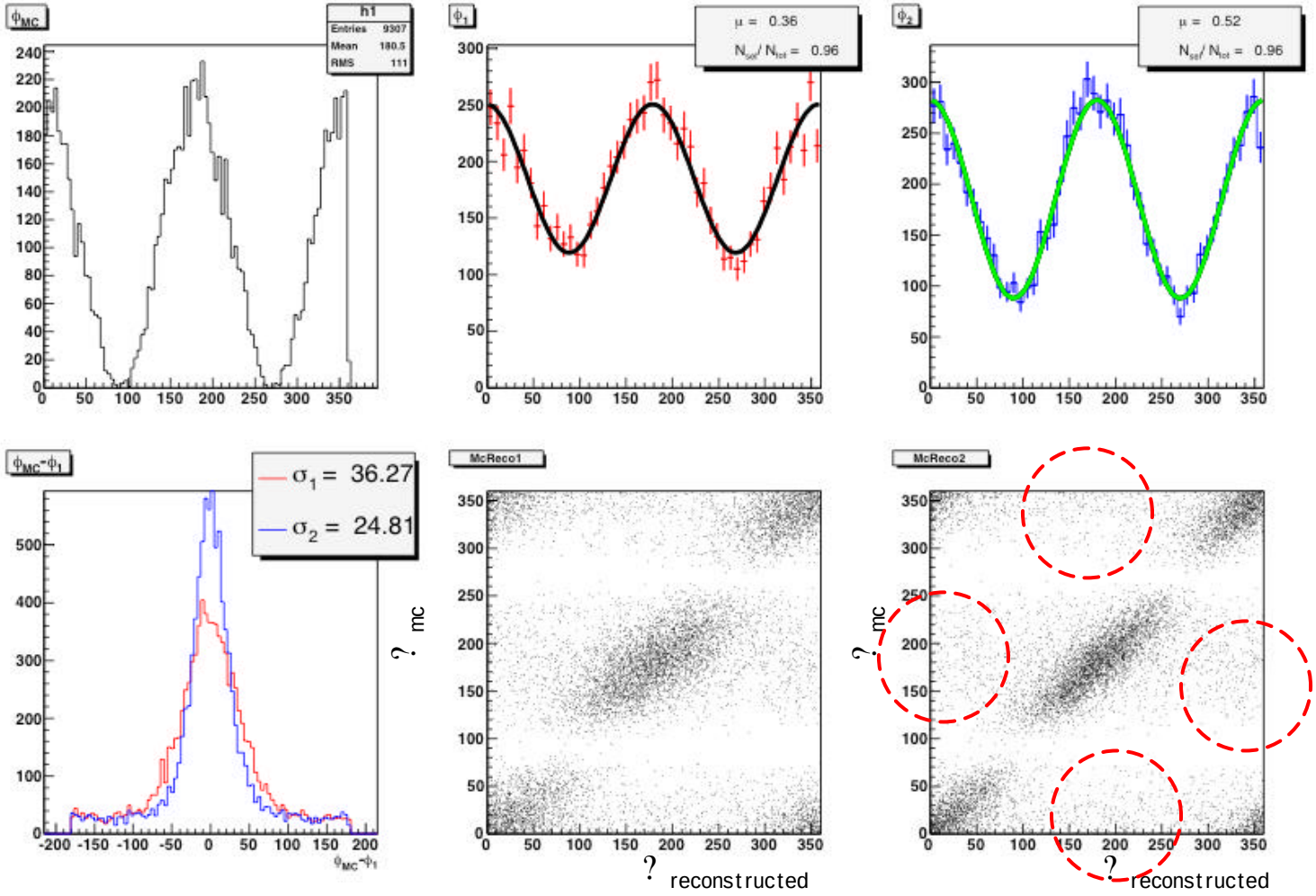

CF4-DME 20-80, 0.5 atm, 6 keV

180 º error in angular reconstruction: the Auger electron has been mistaken for the Bragg peak

Garfield simulation results

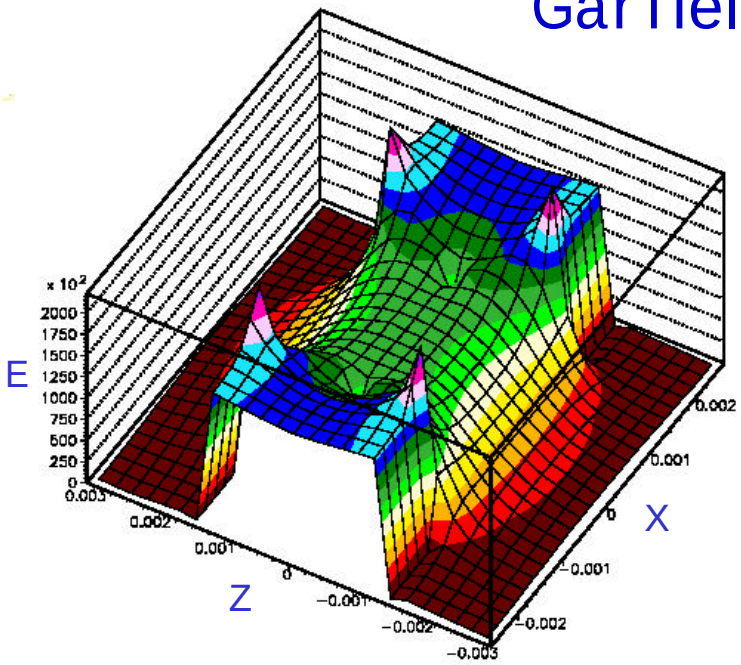

GEM pitch – 50 ?m
GEM thickness – 25 ?m
Drift gap – 6 mm
Collection gap – 1 mm
80 % Ne-20% DME

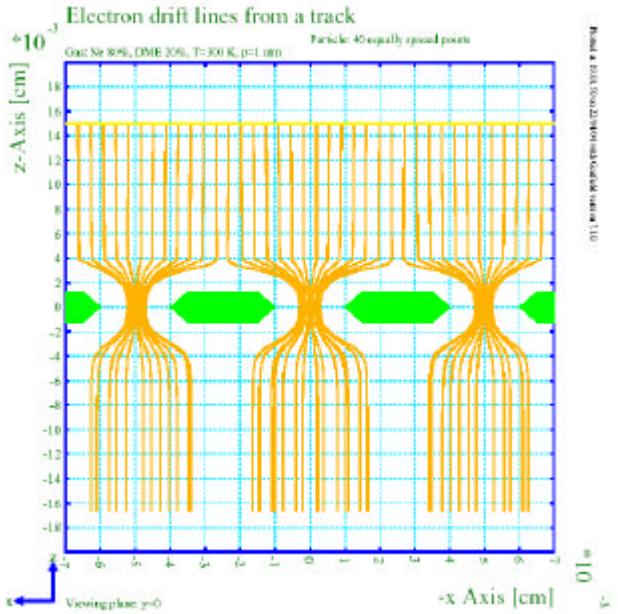

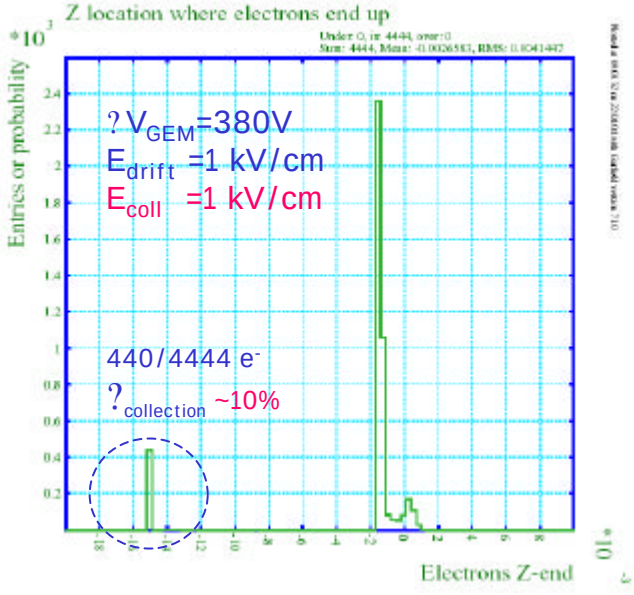

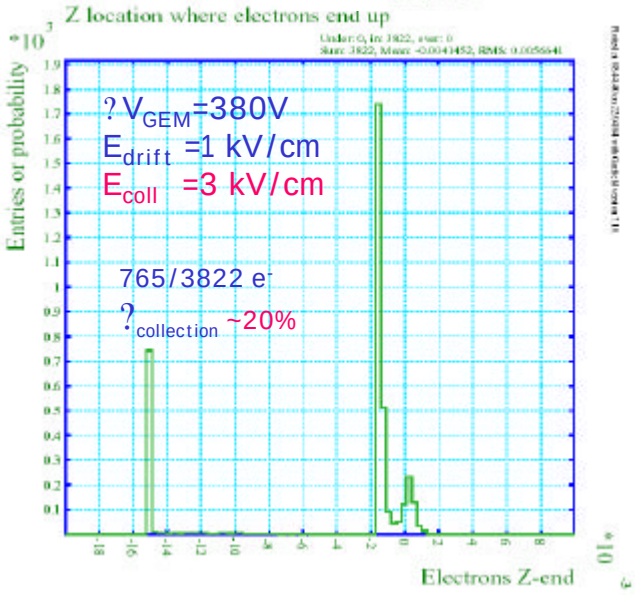

Gain$_{GEM}$? 4000

Angular reconstruction

Angular accuracy vs. *shape*

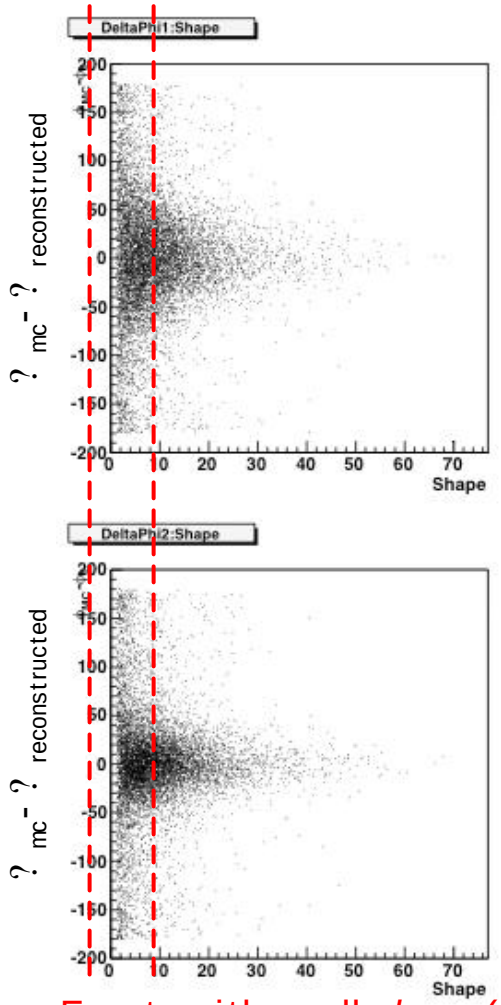

Angular accuracy vs. M_3

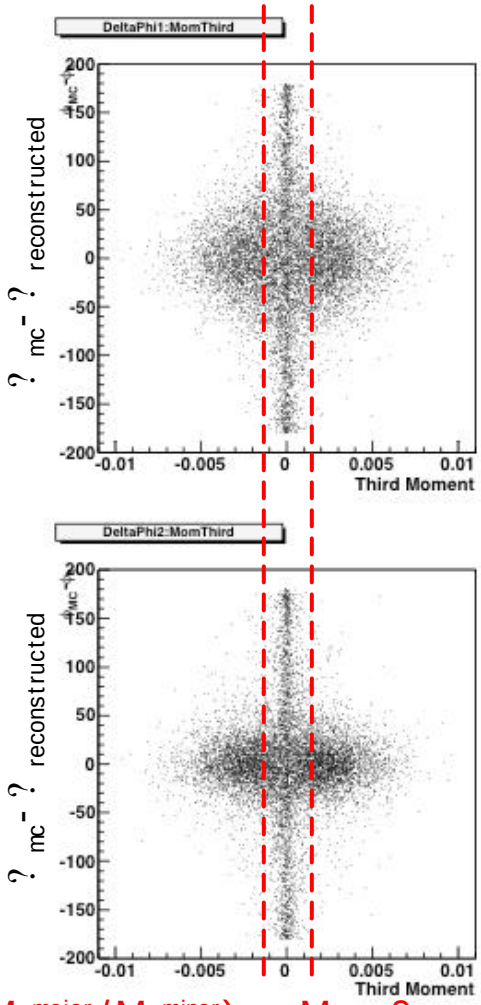

Angular response function

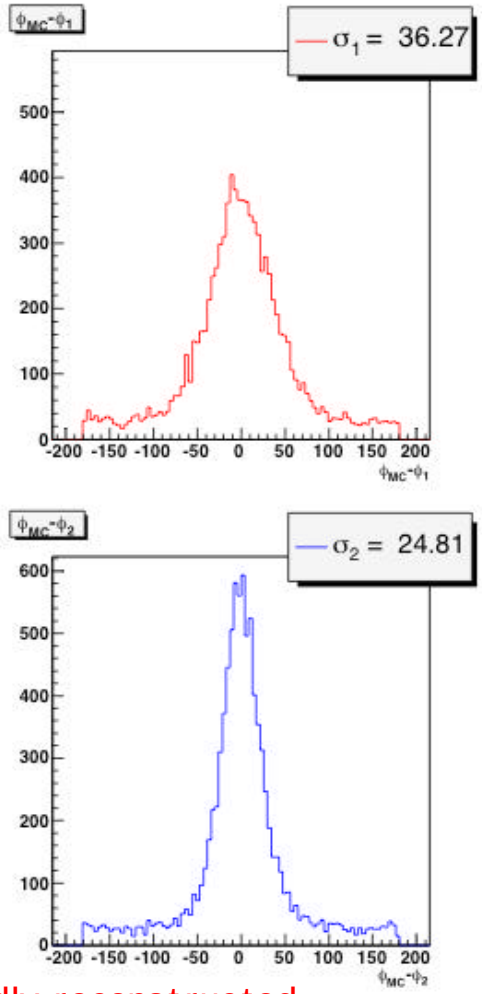

Basic algorithm

Second iteration

Events with small *shape* (M_2^{major}/M_2^{minor}) or $M_3 \sim 0$ are badly reconstructed

CF4-DME 20-80, 0.5 atm, 6 keV

Cuts efficiency

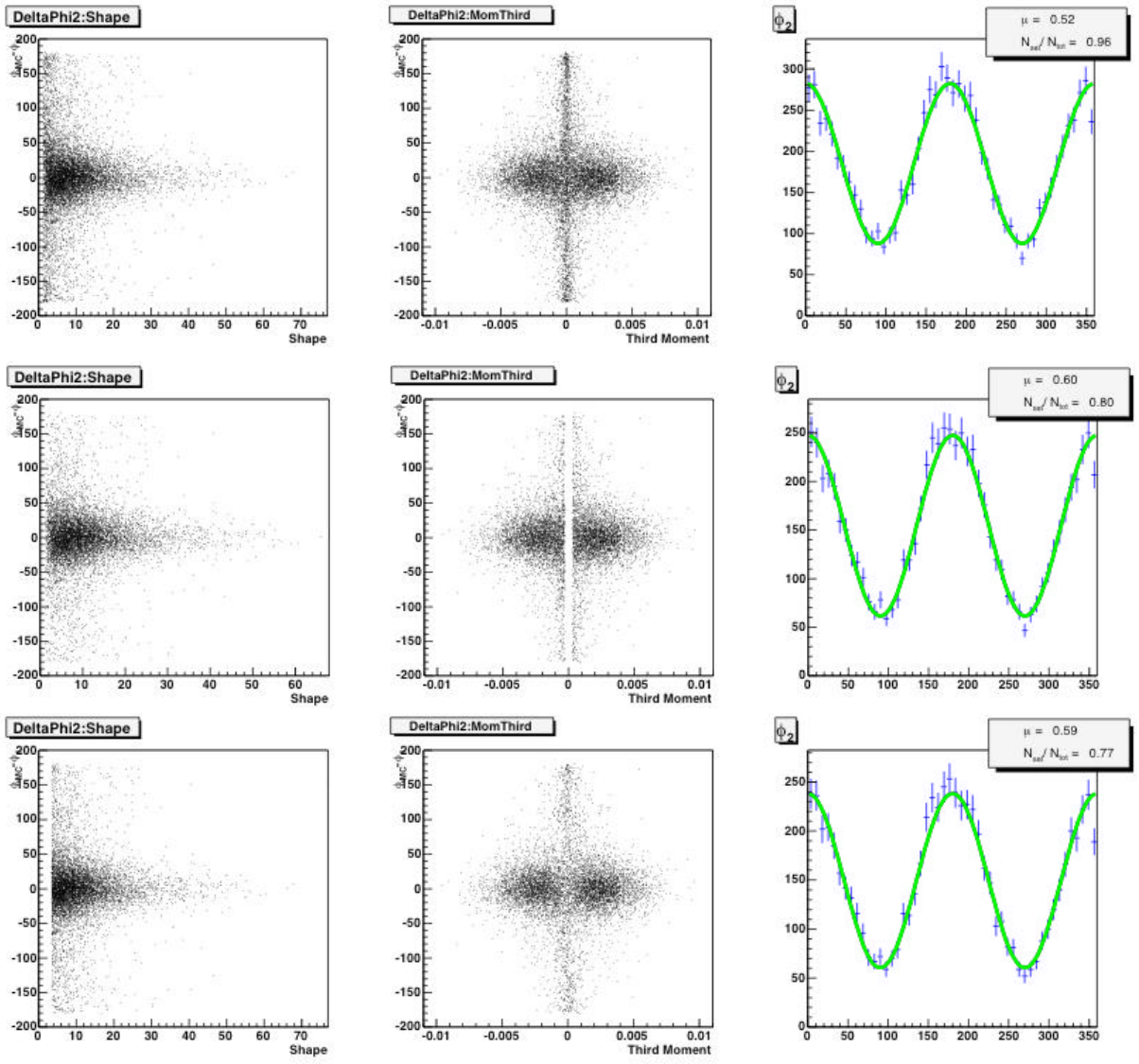

96% of events
? = 0.52

Cut on the *third moment*
80 % of events
? = 0.60

Cut on the *shape*
77 % of events
? = 0.59

CF4-DME 20-80, 0.5 atm, 6 keV

CF4/DME 20-80 0.5 atm 6keV

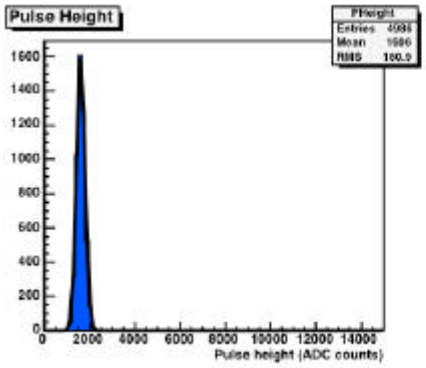

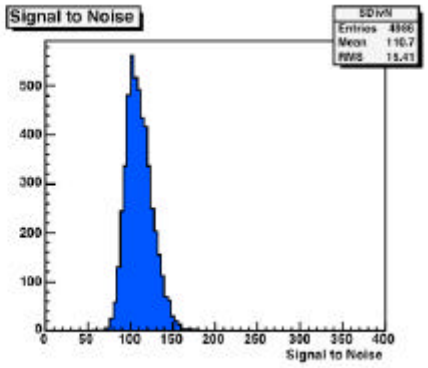

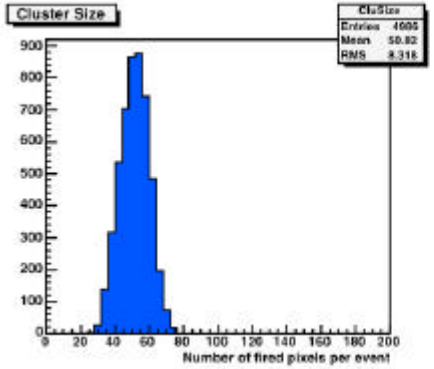

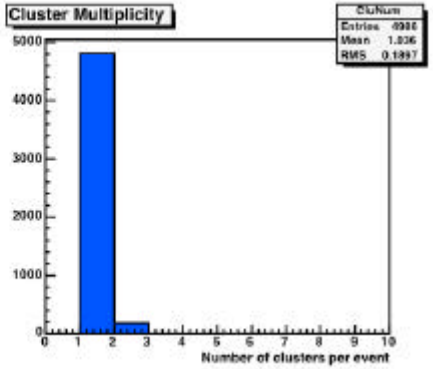

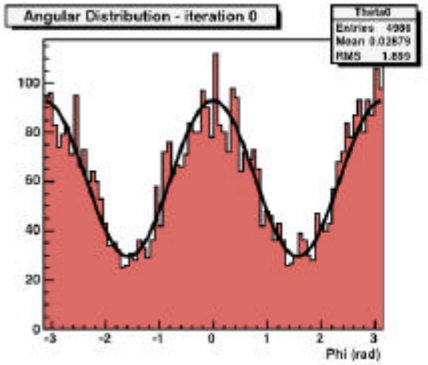

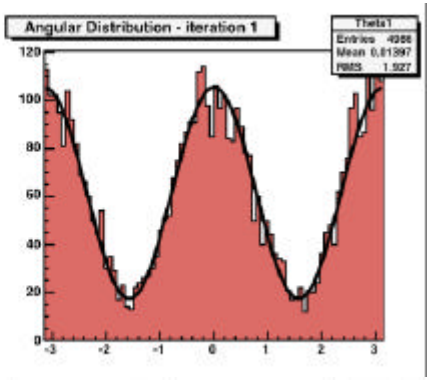

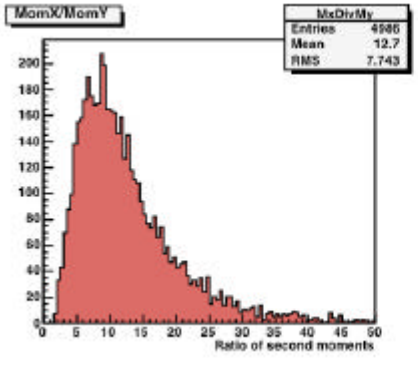

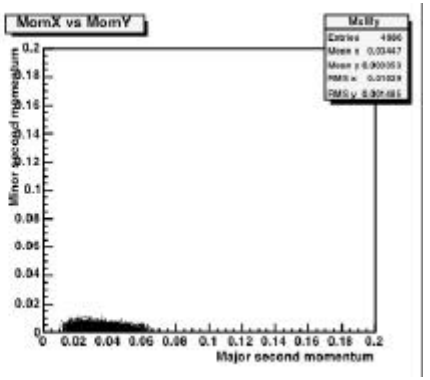

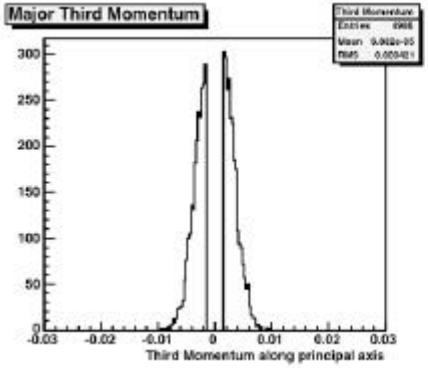

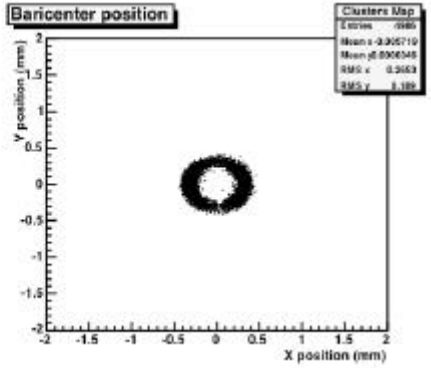

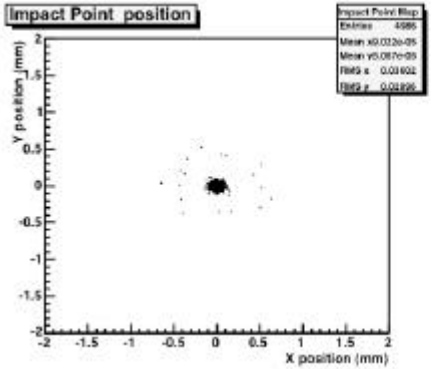

Angular reconstruction - iteration 0:

Modulation factor (%):	51.71	± 1.92
Polarization Angle (degrees):	0.53	± 1.09
Reduced ChiSquare:	1.08	

Angular reconstruction - iteration 1:

Modulation factor (%):	71.71	± 1.66
Polarization Angle (degrees):	0.13	± 0.75
Reduced ChiSquare:	0.91	

Energy Resolution (% FWHM): 27.05

Polarimetric sensitivity: Figure of Merit

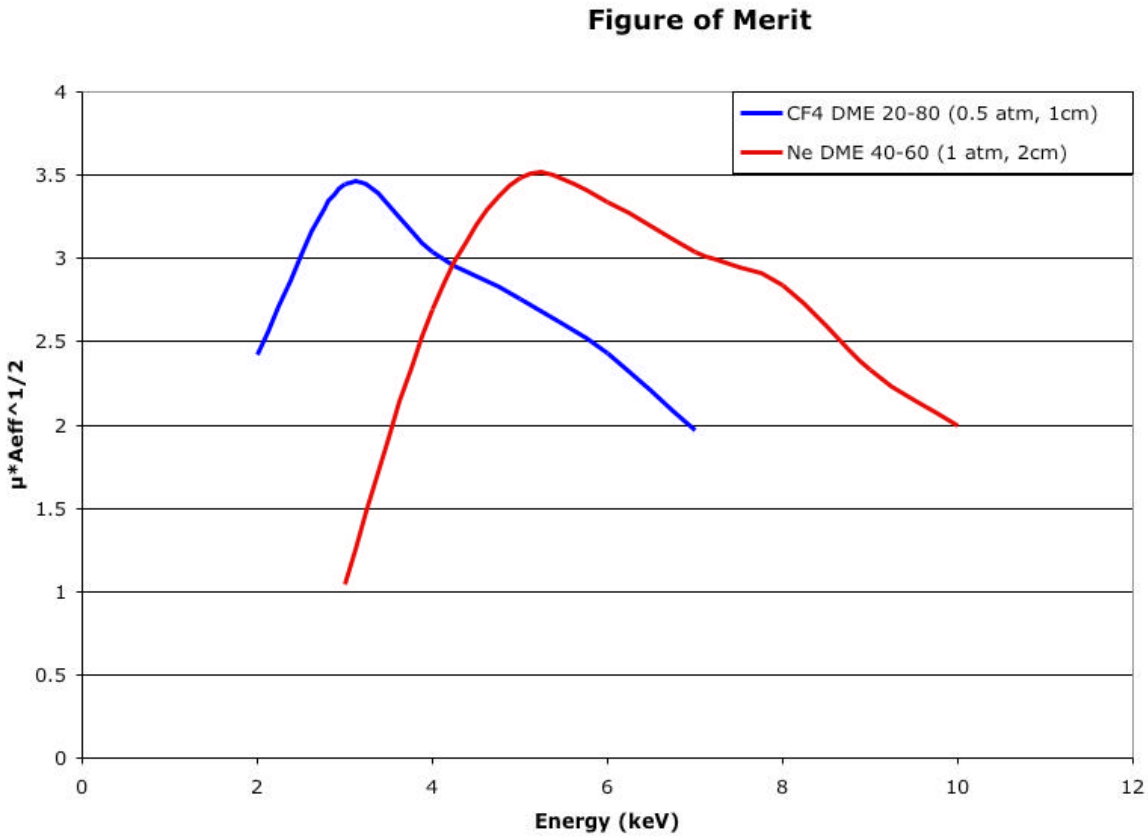

$$FoM \propto (A_{eff})^{1/2}$$

The figure of merit is a measure of the intrinsic capability to measure polarization.

Dependence of polar angle of photo-electron in Ne

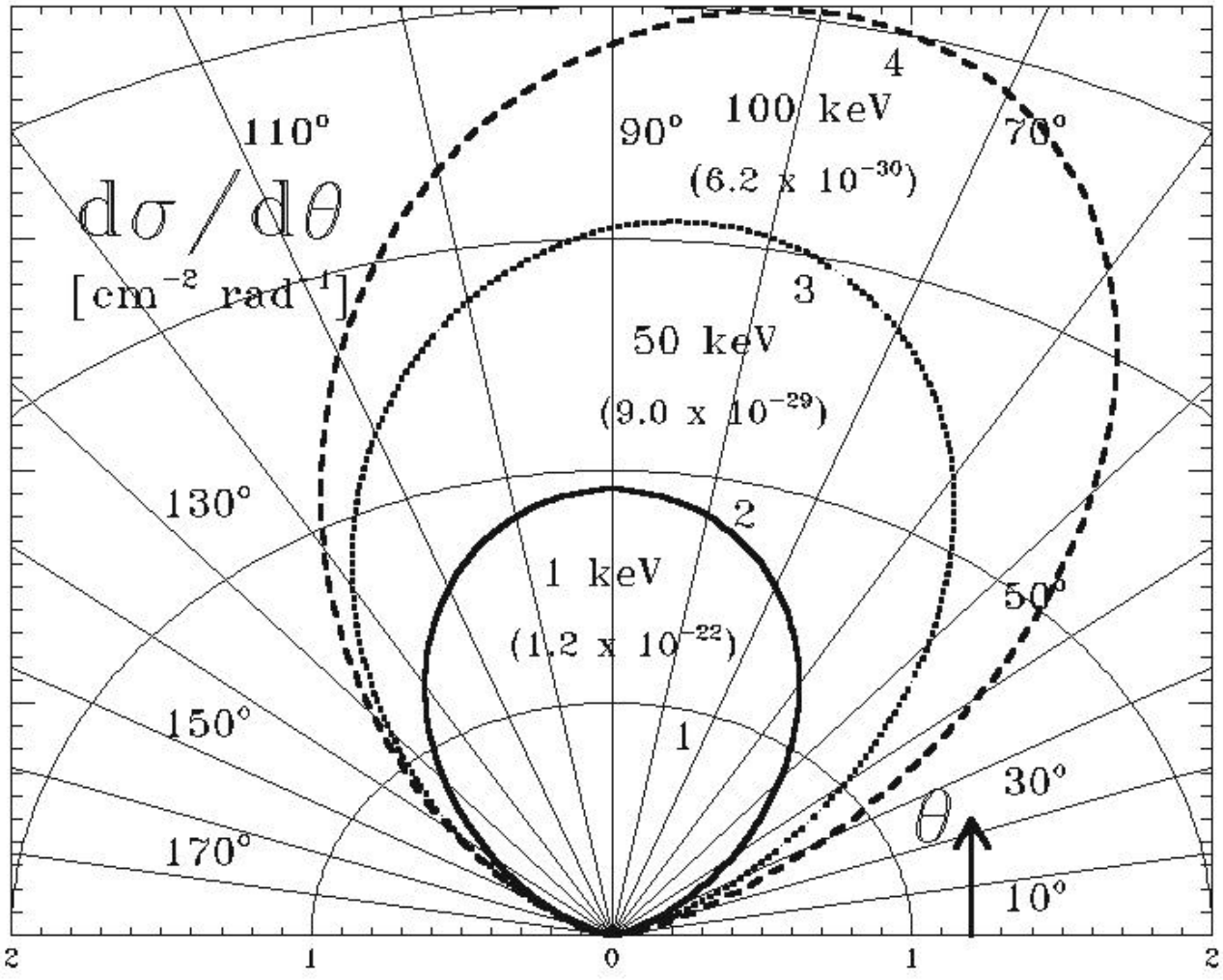

Rise time analysis in gaseous detectors

The rise-time of a signal of a proportional counter is related to the photoelectron emission angle with respect to the anode direction

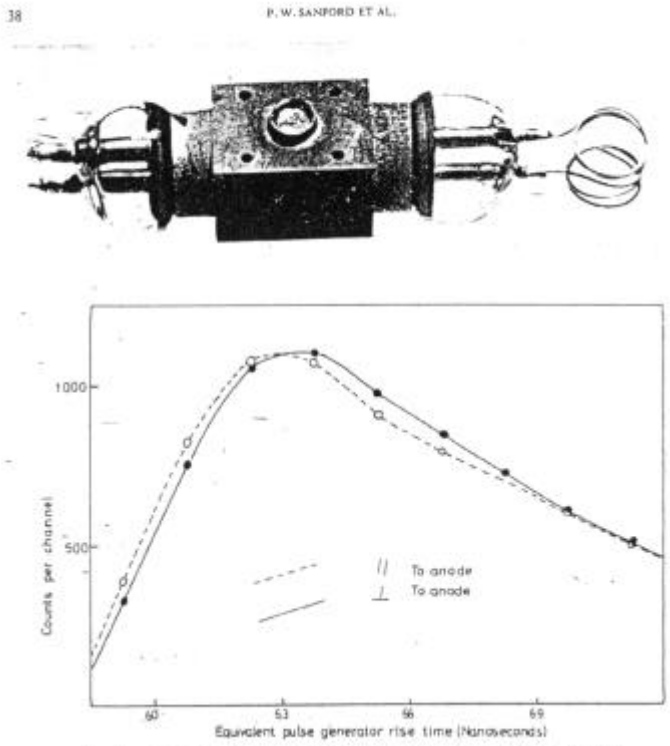

Fig. 7. Pulse rise time distributions for polarized 16.5 keV X-rays.

Sanford et al., 1970

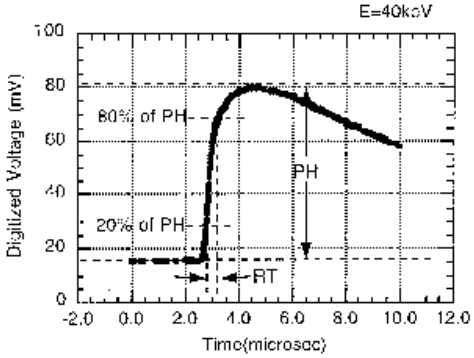

Fig. 4. Signal from the pre-amplifier of the Xe gas proportional counter sampled with the digital oscilloscope. Incident X-ray energy is 40 keV. We reduce the data of each signal pulse into PH (pulse height) and RT (rise time).

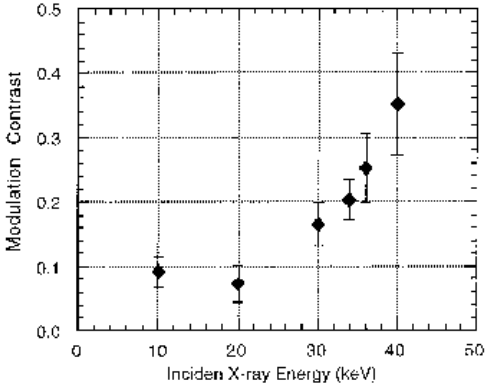

Fig. 8. Modulation contrast for the rise-time polarimeter derived from our experiment. $M = \{\overline{RT}(\Theta = 90^\circ) - \overline{RT}(\Theta = 0^\circ)\}/2\tilde{\sigma}_{RT}/P_{beam}$, where $\tilde{\sigma}_{RT} = \sqrt{\{\sigma^2_{RT}(\Theta = 0^\circ) + \sigma^2_{RT}(\Theta = 90^\circ)\}/2}$, σ_{RT} denotes the standard deviation of the rise time distribution, $\overline{RT}$ is the average rise time, and P_{beam} is the polarization degree of the incident beam (Fig. 2).

Hayashida et al., 1999

1D charge imaging with a Micro-Gap Chamber

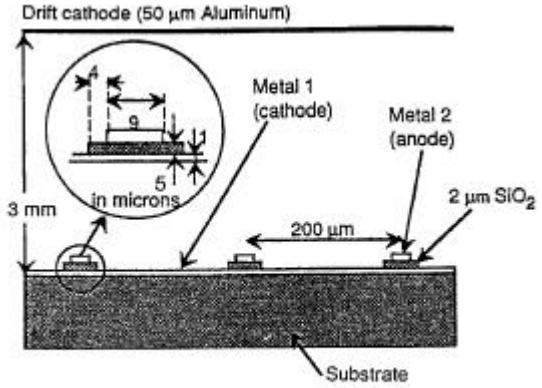

Fig. 1. Sketch of the microgap used in the experiment.

The cluster size is related to the photoelectron emission angle with respect to the anode direction

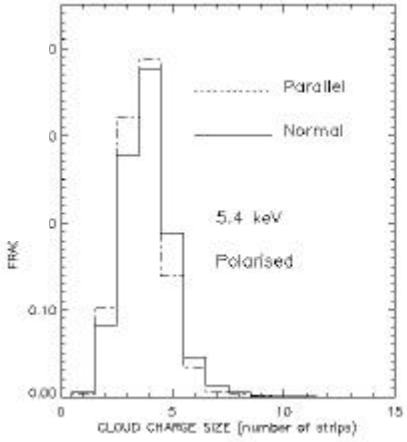

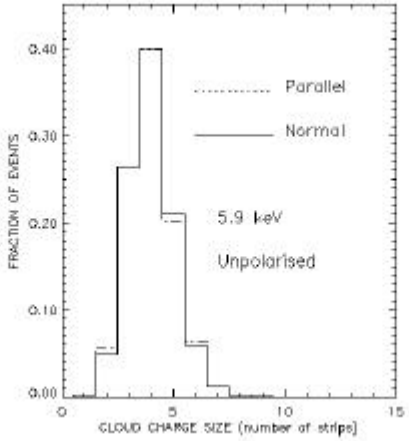

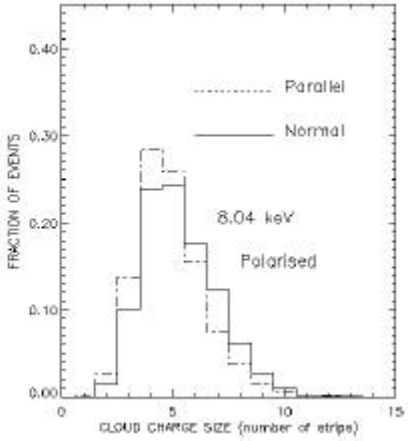

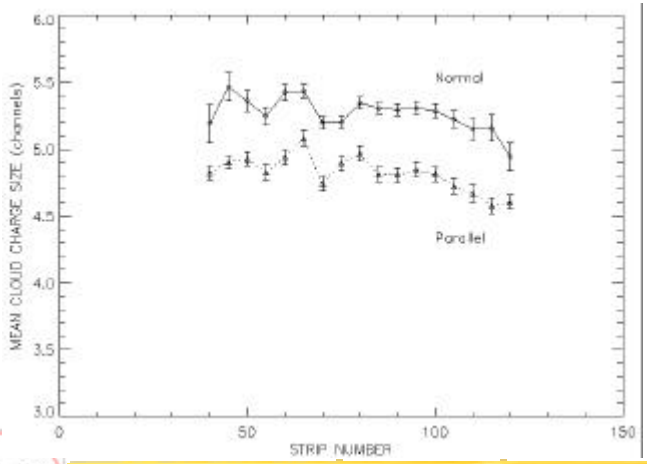

Dependence of mean cluster size on detector orientation (with respect to the polarization direction)

Soffitta al., 1995, 2001

Full detector simulation

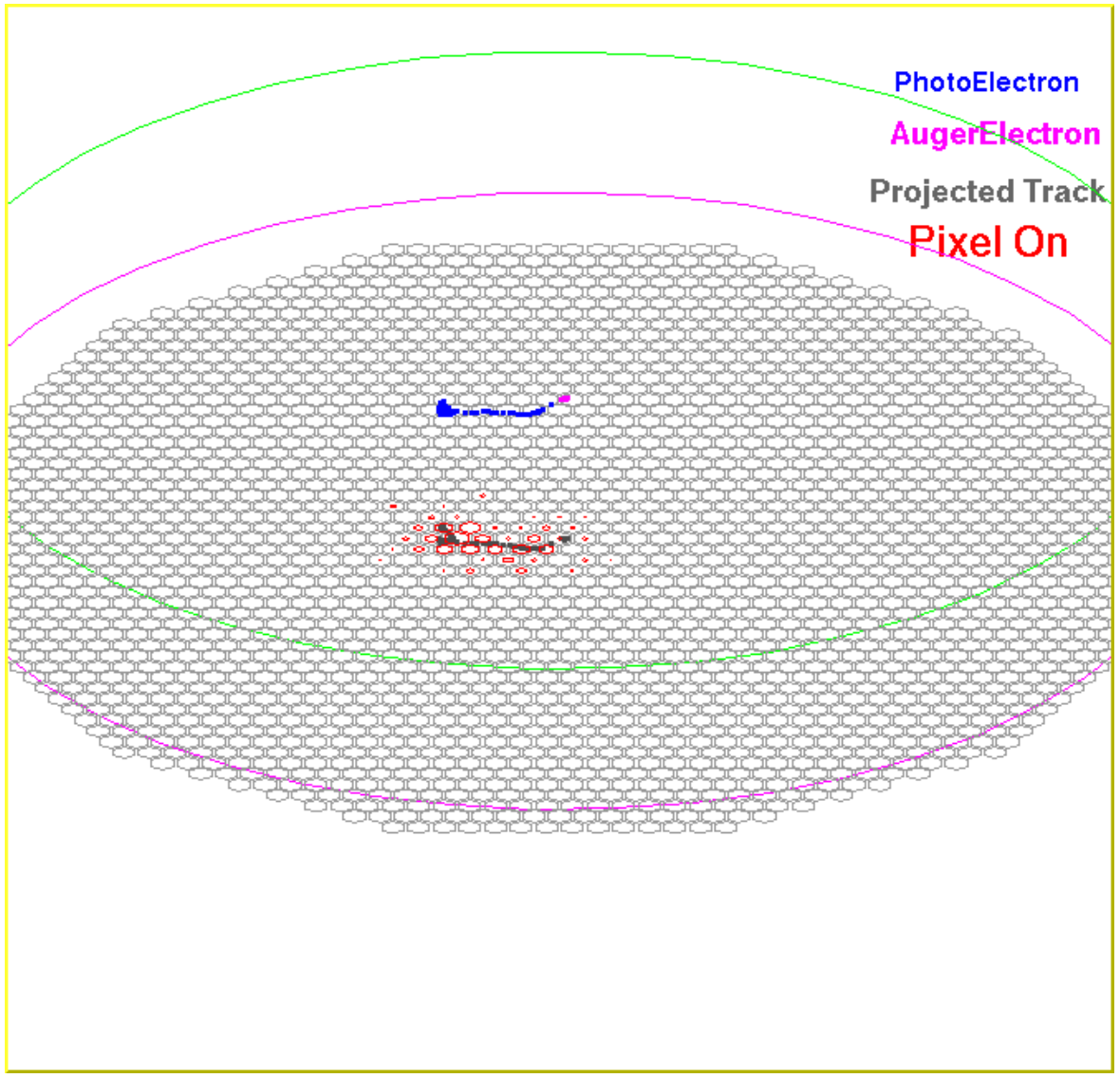

Pixel Event read-out timing

Symbol	Parameter	Min	Typ	Max	Unit
Tpk	Shaper peaking time	3	4	5	us
Tdh	Delay between incoming event & rising edge of MaxHold	0		2	us
Tpd	Peak detection mode duration	10		20	us
Tstore	Analog data retention time for a drift during hold mode lower than 0.1fC equivalent input charge)	1			ms

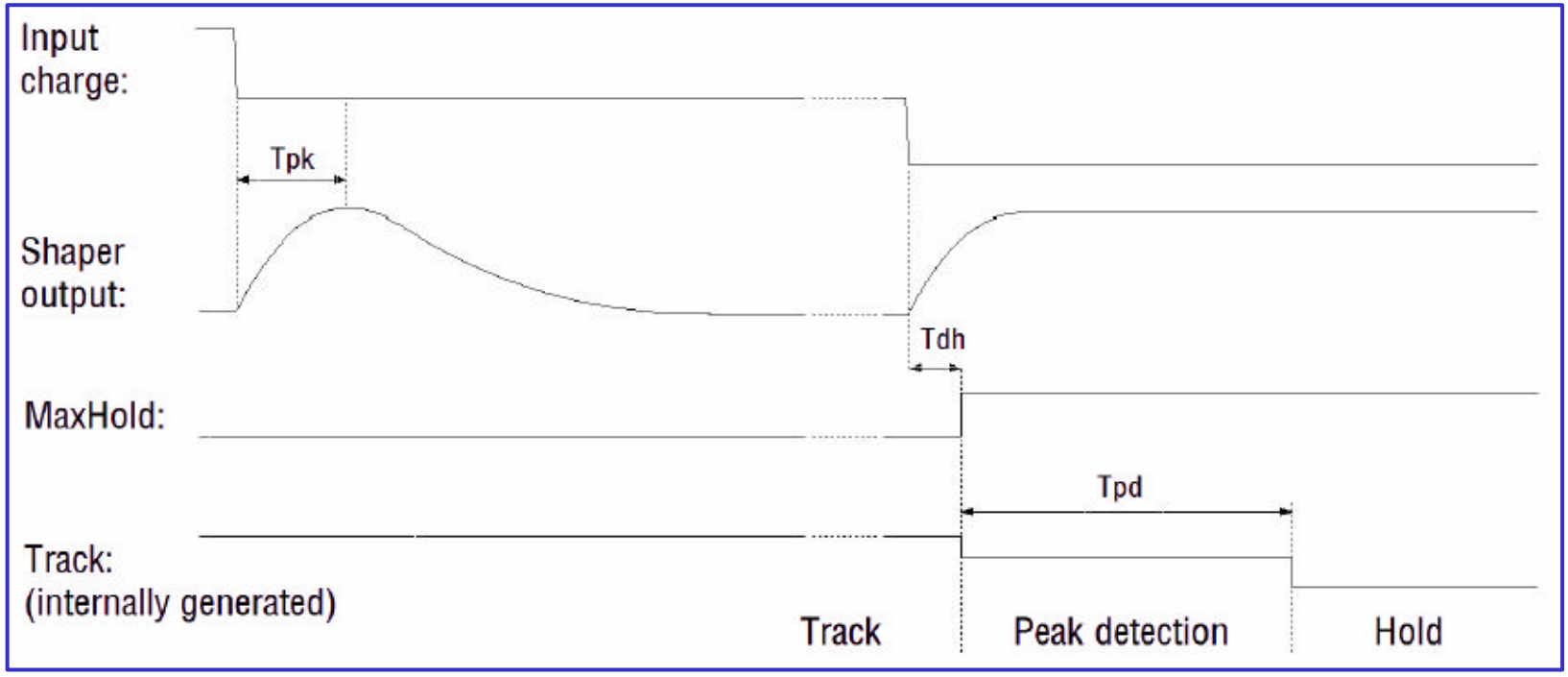

As long as the MaxHold signal is low the shaped pulse of the selected pixel can be observed at the analog output.

Analog out timing characteristics

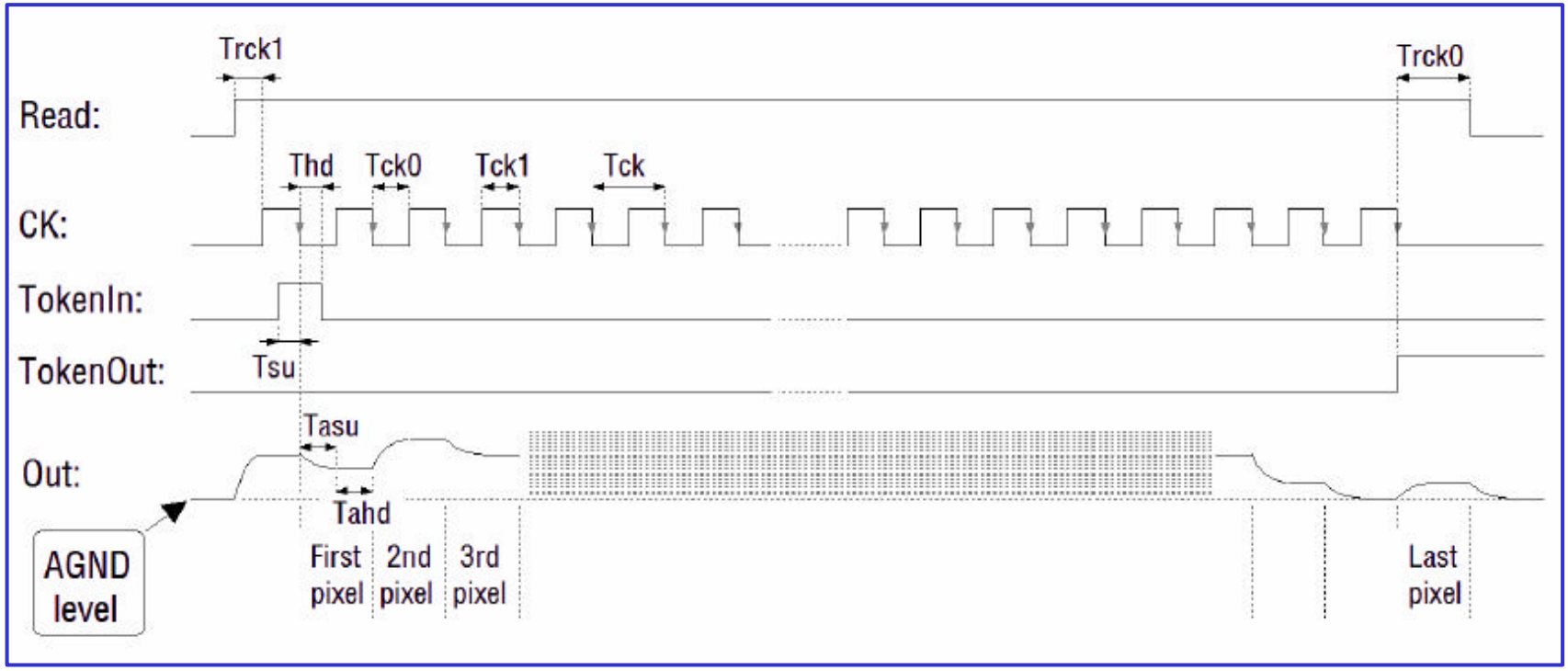

A pixel is selected by introducing a token into the shift register

According to Nature.....

" the work is highly significant for high energy astrophysics and astronomy in general. X-ray polarimetry is a unique probe of particle acceleration in the universe. It will provide a new tool for studying the fascinating and poorly understood jet sources. The instrumentation described here will very likely revolutionize this area of study ....."

letters to nature

An efficient photoelectric X-ray polarimeter for the study of black holes and neutron stars

Enrico Costa*, Paolo Soffitta*, Ronaldo Bellazzini†, Alessandro Brez†, Nicholas Lumb† & Gloria Spandre†

* *Istituto di Astrofisica Spaziale del CNR, Via Fosso del Cavaliere 100, I-00133, Rome, Italy*
† *Istituto Nazionale di Fisica Nucleare-Sezione di Pisa, Via Livornese 1291, I-56010 San Piero a Grado, Pisa, Italy*

The study of astronomical objects using electromagnetic radiation involves four basic observational approaches: imaging, spectroscopy, photometry (accurate counting of the photons received) and polarimetry (measurement of the polarizations of the observed photons). In contrast to observations at other wavelengths, a lack of sensitivity has prevented X-ray astronomy from making use of polarimetry. Yet such a technique could provide a direct picture of the state of matter in extreme magnetic and gravitational fields[1–6], and has the potential to resolve the internal structures of compact sources that would otherwise remain inaccessible, even to X-ray interferometry[7]. In binary pulsars, for example, we could directly 'see' the rotation of the magnetic field and determine if the emission is in the form of a 'fan' or a 'pencil' beam[1,8]. Also, observation of the characteristic twisting of the polarization angle in other compact sources would reveal the presence of a black hole[9–12]. Here we report the development of an instrument that makes X-ray polarimetry possible. The factor of 100 improvement in sensitivity that we have achieved will allow direct exploration of the most dramatic objects of the X-ray sky.

The main advantage of the proposed polarimeter is its capability of investigating active galactic nuclei (quasars, blazars and Seyfert galaxies) for which polarization measurements have been suggested, crucial to understand the geometry and physics of emitting regions. We can separate synchrotron X-rays from jets[13,14] from the emission scattered by the disk corona or by a thick torus. The effects of relativistic motions and of the gravitational field of a central black hole have probably been detected by iron line spectroscopy on the Seyfert-1 galaxy MCG-6-30-15 (ref. 15) but this feature is not ubiquitous in active galactic nuclei. Polarimetry of the X-ray continuum provides a more general tool to explore the structure of emitting regions[16,17], to track instabilities and to derive direct information on mass and angular momentum[12] of supermassive black holes.

In spite of this wealth of expectations, the important but only positive result until now is the measurement, by the Bragg technique, of the polarization of the Crab nebula[18,19]. The Stellar X-ray Polarimeter[20] (SXRP) represents the state of the art for conventional methods based on Bragg diffraction and Thomson scattering. However, Bragg polarimetry[21] is dispersive (one angle at one time) and very narrow-band. Thomson polarimetry[22] is non-imaging and band-limited (>5 keV). This limits the sensitivity of SXRP to a few bright, galactic sources only.

The photoelectric effect is very sensitive to polarization. The electron is ejected from an inner shell with a kinetic energy which is the difference between the photon energy and the binding energy. The direction of emission is not uniform but is peaked around that of the electric field of the photons (see Fig. 1a). This photoelectron

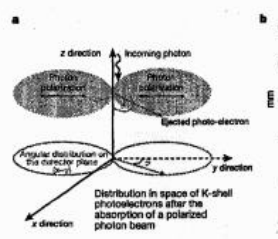

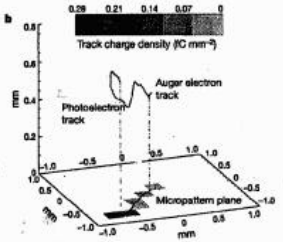

Figure 1 Basic physics of the photoelectric effect in gas. a, Following the photon conversion in the gas, the photoelectric effect. The photoelectron is ejected in directions that carry a significant memory of the electric field of the photon. When the beam is linearly polarized the electrons are ejected preferentially around the electric field. The cross-section of *s* electrons is:

$$\frac{\partial\sigma}{\partial\Omega} = r_e^2 \frac{Z^4}{137^4}\left(\frac{mc^2}{h\nu}\right)^{7/2}\frac{4\sqrt{2}\sin^2(\theta)\cos^2(\varphi)}{(1-\beta\cos(\theta))^4}$$

where r_e is the classical electron radius, Z is the atomic number of the target material and β is the electron velocity, as a fraction of the speed of light c. The figure shows the emission angle θ and azimuth angle φ. b, A simulated 6-keV photoelectron and Auger track, showing propagation in the gas and collection on a plane with sensitivity to both energy and position. The photoelectron is slowed by ionizing collisions with outer electrons of the atoms of the medium. The energy loss increases with decreasing kinetic energy (Bethe law for low energy).

$$\frac{\partial E}{\partial x} \propto \frac{1}{\beta^2} \propto \frac{1}{E_{kin}}$$

Electrons are also scattered by charges in the nuclei with no significant energy loss. This follows the screened Rutherford law:

$$\frac{\partial\sigma}{\partial\Omega} \propto \frac{Z^4/E_{kin}^2}{(\sin^2(\delta/2)+\alpha_{screen})^2}$$

Whereas scattering crucially depends on the atomic number, slowing down is only moderately dependent. The primary ionizations are then projected onto the sense plane. The charge density in each pixel is proportional to the energy loss, and is therefore related to the electron kinetic energy. The first part of the photoelectron path has a lower charge density, but it is closer to the initial direction of the photoelectron and so also closely related to the photon polarization direction. The second part has a higher charge density but it is randomized. The Auger electron track does not bring information on polarization.

Noise measurement

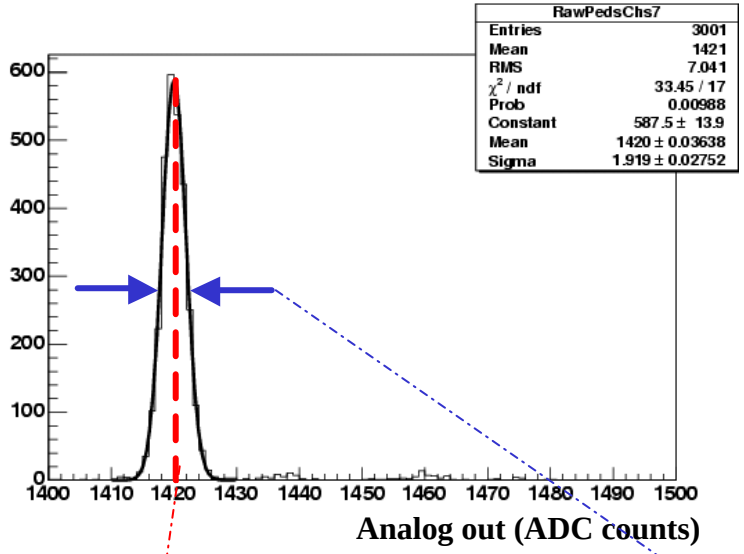

Single channel analog output (few k random triggers)

Noise RMS: ~ 100 e⁻ ENC (electronics gain is ~ 100 mV/fC): sensitive to the single primary electron with a gas gain < 1000 (easily achievable with a single GEM).

Pedestal

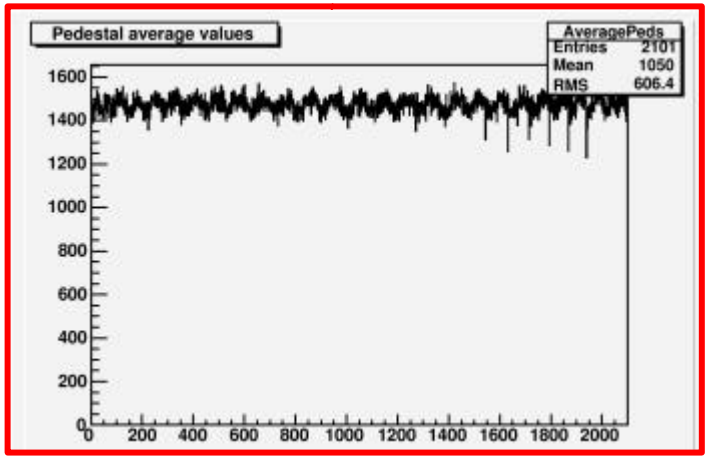

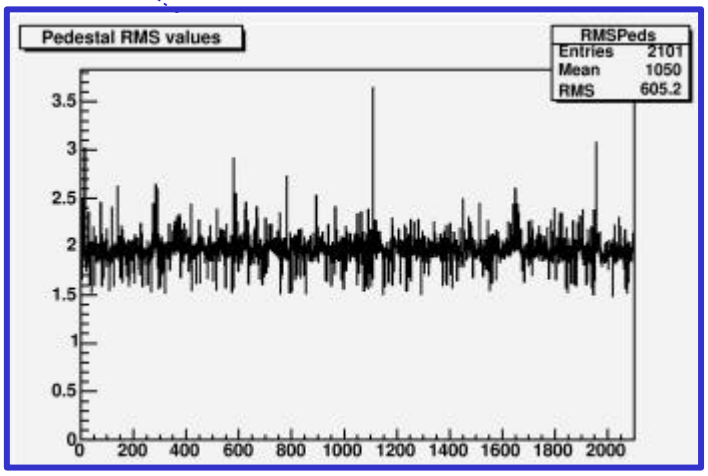

Channel response uniformity and X-talk